

# Yarkovsky origin of the unstable asteroids in the 2/1 mean motion resonance with Jupiter

M. Brož<sup>1\*</sup>, D. Vokrouhlický<sup>1\*</sup>, F. Roig<sup>2\*</sup>, D. Nesvorný<sup>3\*</sup>, W.F. Bottke<sup>3\*</sup>,  
and A. Morbidelli<sup>4\*</sup>

<sup>1</sup>*Institute of Astronomy, Charles University, Prague, V Holešovičkách 2, 18000 Prague 8, Czech Republic*

<sup>2</sup>*Observatório Nacional - MCT, Rua Gal. José Cristino 77, Rio de Janeiro, 20921-400 RJ, Brasil*

<sup>3</sup>*Department of Space Studies, Southwest Research Institute, 1050 Walnut St., Suite 400, Boulder, CO 80302, USA*

<sup>4</sup>*Observatoire de la Côte d’Azur, Dept. Cassiopee, BP 4224, 06304 Nice Cedex 4, France*

Accepted ???, Received 1 March 2005

## ABSTRACT

The 2/1 mean motion resonance with Jupiter, intersecting the main asteroid belt at  $\approx 3.27$  AU, contains a small population of objects. Numerical investigations have classified three groups within this population: asteroids residing on stable orbits (i.e., Zhongguos), marginally stable orbits with dynamical lifetimes on the order 100 My (i.e., Griquas) and unstable orbits. In this paper, we reexamine the origin, evolution and survivability of objects in the 2/1 population. Using recent asteroid survey data, we have identified one hundred new members since the last search, which increases the resonant population to 153. The most interesting new asteroids are those located in the theoretically-predicted stable island A, which until now had though to be empty. Next, we investigated whether the population of objects residing on the unstable orbits could be resupplied by material from the edges of the 2/1 resonance by the thermal drag force called the Yarkovsky effect (and the YORP effect, which is related to the rotational dynamics). Using  $N$ -body simulations, we showed that test particles pushed into the 2/1 resonance by the Yarkovsky effect visit the same regions occupied by the unstable asteroids. We also found that our test bodies had dynamical lifetimes consistent with the integrated orbits of the unstable population. Using a semi-analytical Monte-Carlo model, we computed the steady-state size distribution of magnitude  $H < 14$  asteroids on unstable orbits within the resonance. Our results provide a good match with the available observational data. Finally, we discuss whether some 2/1 objects may be temporarily-captured Jupiter family comets or near-Earth asteroids.

**Key words:** celestial mechanics – minor planets, asteroids – methods: numerical.

## 1 INTRODUCTION

In 1869 the first asteroid, 108 Hecuba, was found to reside near the 2/1 mean motion resonance with Jupiter (Luther 1869; Tietjen 1869). (Hereafter, we denote this resonance as J2/1, with other resonances denoted accordingly.) Since that time, asteroidal dynamics near or inside mean motion resonances with Jupiter have attracted attention. For example, Hansen, Bohlín and von Zeipel were among the first in a long list of researchers who tried to deal with the difficulties of insufficient convergence of the resonant trigonometric perturbation series for Hecuba-like orbits (historical notes in Hagihara 1975). These cases demonstrated the limits

of analytical methods (e.g., perturbation theory). More recently, semi-analytical and numerical methods have allowed to make great progress in our understanding of resonant dynamics. In particular, we can now decipher some of the minute details of asteroid motion inside the J2/1 (e.g. Murray 1986; Henrard & Lemaître 1987; Lemaître & Henrard 1990; Morbidelli & Moons 1993; Ferraz-Mello 1994; Henrard et al. 1995; Morbidelli 1996; Nesvorný & Ferraz-Mello 1997; Moons et al. 1998; Morbidelli 2002).

Although today we recognize that Hecuba itself is just outside the J2/1, we know that more than hundred asteroids reside *inside* the J2/1. This sample is large enough to allow us to quantitatively analyse their origin. Recently, Roig et al. (2002) published a catalogue of 53 asteroids residing in the J2/1 and placed them into 3 groups according to their dynamical lifetime in the resonance ( $t_{J2/1}$ ). Half of the orbits

\* E-mail: mira@sirrah.troja.mff.cuni.cz (MB); froig@on.br (FR); vokrouhl@cesnet.cz (DV); davidn@boulder.swri.edu (DN); morby@obs-nice.fr (AM); bottke@boulder.swri.edu (WFB)

were found to be stable ( $t_{J2/1} \approx 1$  Gy), much like that of (3789) Zhongguo, the first stable asteroid discovered in the J2/1 resonance. The remaining bodies are either marginally stable ( $t_{J2/1} \approx 100$  My) or unstable ( $t_{J2/1} \approx 10$  My), with the leading asteroids in each group being (1362) Griqua and (1922) Zulu. Importantly, the largest asteroids of all three groups are between  $D = 20 - 30$  km in diameter.

Asteroidal sizes and dynamical lifetimes are very basic indicators of their origin. We know that unstable resonant asteroids are not primordial because they cannot reside on their current orbits for 4.6 Gy.<sup>1</sup> Moreover, small asteroids are unlikely to survive 4.6 Gy of collisional evolution. Bottke et al. (2004) estimate the collisional lifetimes of  $D < 10$  km asteroids are less than the age of the Solar system.

The situation is different for asteroidal populations inside the J3/2 (the so called Hilda group) and in the J4/3 (the Thule group). The dynamical lifetimes of their members tend to be long (e.g. Nesvorný & Ferraz-Mello 1997), while the largest observed asteroids are substantially larger ( $D = 170$  km and 125 km respectively) than those in the J2/1 ( $D = 20 - 30$  km). Given that these objects are big and their eccentric orbits cross only a portion of the main belt (e.g. Dahlgren 1998), their collisional lifetimes are definitely larger than the age of the Solar system. As a consequence, the Hilda and Thule groups are likely to be primordial.

There are two end-member cases to explain the origin of the J2/1 population:

- (i) The population is far from steady state, such that the observed objects were produced by a recent disruption event (*instantaneous-injection model*), or
- (ii) The population is in steady state and we need to find the process that sustains it (*continuous-flow model*).

It is also possible that both cases are partially correct, and that different resonant groups have different origins.

In the 1990's, the preferred hypothesis was type (i). Here the resonant asteroids were fragments injected into the J2/1 during the Themis family formation event (e.g. Morbidelli et al. 1995; Moons et al. 1998). Recent asteroid family results, however, suggest this possibility is unlikely. Numerical simulations of large break-up events in the asteroid belt predict escape velocities significantly smaller than would be needed to directly inject asteroids into the J2/1 (Michel et al. 2001; in fact, characteristic velocities are too small to populate the currently observed family outside the resonance). In addition, there are several lines of evidence to suggest that prominent asteroid families like Koronis (Vokrouhlický et al. 2003) or Themis are several Gy old (Morbidelli et al. 2003; Bottke et al. 2004). Such ages are incompatible with the relatively short dynamical lifetimes of the Griquas and unstable resonant asteroids. On the other hand, Roig et al. (2002) argue that the steep size distribu-

tion seen among the Zhongguos (i.e., the stable J2/1 objects) may be more consistent with a recent collisional origin.

At first glance it might seem possible, that the majority of the unstable asteroids were produced by a *recent* catastrophic disruption event, with some of the fragments directly injected into the J2/1. Although the stochastic nature of such events make it difficult to rule this scenario out *a priori*, we believe the available evidence suggests that most J2/1 asteroids are unlikely to have formed by this process, mainly because the dynamical lifetime of most unstable asteroids is of the order 10 My and this time-scale implies that a collisional event capable of injecting fragments into the J2/1 should have leave behind an observable asteroid family along the J2/1 border. As described in Nesvorný et al. (2003), it is now possible to systematically search for clusters of bodies in proper element space using a database of more than 100,000 asteroids computed by A. Milani and Z. Knežević (e.g. Knežević et al. 2003). Though the outer main belt is more observationally incomplete than the inner main belt, Nesvorný et al. (2003) found no evidence for new families along the J2/1 border. This limits the size of any potentially-disrupted parent bodies to objects smaller than Karin, a  $D \simeq 30$  km asteroid that disrupted and produced a small cluster of fragments in the Koronis asteroid family 5.8 My ago (Nesvorný et al. 2002b; Nesvorný & Bottke 2004). Because some unstable asteroids are comparable in size to the Karin parent body, it appears that Karin-sized disruption events cannot produce the largest unstable asteroids. For smaller unstable asteroids, we can use the limits provided by the Karin cluster to estimate, in a back-of-the-envelope fashion, whether they could have been produced by a recent breakup event. Here we assume the unstable asteroids were the by-product of a recent disruption among one of the  $D = 20 - 30$  km asteroids bordering the J2/1. As shown by Nesvorný et al. (2002b), the Karin disruption event ejected km-sized fragments at velocities of  $\leq 15$  m/s, with the maximum distance reached by the observed fragments from the centre of the family being  $\Delta a \simeq 0.005$  AU. This constrains our putative forming event for the unstable asteroids to a distance of 0.005 AU or smaller from the J2/1 border. Searching main belt orbital elements, we find that only  $\simeq 1\%$  of  $D = 20 - 30$  km asteroids fulfil this criterion. If the time interval between  $D = 20 - 30$  km disruption events across the whole main belt is  $\simeq 10$  My (Bottke et al. 2004), there is only a 0.5 – 3% chance that such an event occurred near the J2/1 border within the dynamical lifetime of the unstable asteroids (5 – 30 My). Given these odds and the lack of evidence for any recent family-forming events near the J2/1, we conclude that most unstable asteroids were not produced by a collisional injection.

Alternatively, the current view of asteroid family evolution, namely that the initial break-up event was followed by a subsequent dynamical spreading due to the effect of the Yarkovsky forces and chaos in weak resonances (e.g. Bottke et al. 2001; Nesvorný et al. 2002a; Bottke et al. 2003), offers a natural continuous-flow model of type (ii) mentioned above. As asteroids slowly diffuse in semimajor axis over time, they can reach the border of a resonance and fall into it. This scenario provides a continuous resupply of resonant asteroids (dominated by the Yarkovsky effect), and is supported by observations of asteroids on highly unstable orbits adjacent to the resonances (e.g. Milani & Farinella 1995; Vokrouh-

<sup>1</sup> Besides that, Michtchenko & Ferraz-Mello (1997) and Ferraz-Mello et al. (1998) have pointed out that stability inside the J2/1 might have been significantly reduced early after formation of the Solar system during the migration of giant planets. The period of the Great Inequality in Jupiter's motion could have been closer to the libration period of asteroids inside the J2/1, which would have caused significant depletion of any primordial resonant population.

lický et al. 2001; Guillens et al. 2003) and by a quantitative model of the transport of near-Earth asteroids (NEAs) from the main belt (Morbidelli & Vokrouhlický 2003).

In this paper, we show the continuous-flow of asteroids driven by the Yarkovsky effect may explain the presence of unstable asteroids in the J2/1 (as already suggested by Roig et al. 2002). We note that Tsiganis et al. (2003) developed a similar model for the small unstable population in the J7/3, where the asteroids are resupplied from the Koronis and Eos families, and Vokrouhlický et al. (2005; in preparation) did comparable work for the J9/4 being visited by members of the Eos family. Because the population of bodies in the J2/1 is substantially larger than in the weaker J7/3 and J9/4, the model for the J2/1 can be tested in a more quantitative way. In fact, our work combines techniques that have been used to explain properties of the NEA population, namely (i) Tracking test bodies from their source region into a target region using numerical integration techniques (e.g. Bottke et al. 2000; Bottke et al. 2002), and (ii) A semi-analytical technique for investigating the steady-state size distribution of bodies in the target region, including the absolute number of objects (e.g. Morbidelli & Vokrouhlický 2003).

In Section 2, we update the observed population in the J2/1. In Secs. 3.1 and 3.2, we describe our numerical and semi-analytical models of Yarkovsky-driven transport from the main belt on to resonant orbits, as well as results from those models. In the Sec. 3.3, we discuss other possible sources of very unstable resonant asteroids in the J2/1.

## 2 UPDATE OF THE RESONANT POPULATION

Our first task is to update the known population of asteroids inside the J2/1. Note that a preliminary analysis which included a more detailed description of some of our techniques was reported in Brož et al. (2004). We find many new asteroids have been discovered in the J2/1 since the work of Roig et al. (2002), with most of the new data provided by NEA survey systems like LINEAR, Spacewatch, NEAT, LONEOS, etc. (e.g. Stokes et al. 2003). Moreover, refined orbital identification techniques make the orbits more accurate than in the past (e.g. Milani et al. 2001). We discuss the new objects below.

### 2.1 Pseudo-proper resonant elements

In order to identify and classify resonant asteroids, we need to properly characterize their orbits. However, the osculating orbital elements (including semimajor axis) undergo large changes inside the resonance due to planetary perturbations, and their elimination requires a different technique than that used in the case of non-resonant asteroids (e.g. Knežević et al. 2003) — the averaging over a fundamental variable is not possible here. In the case of J2/1, we have the resonance critical angle defined as

$$\sigma = 2\lambda_J - \lambda - \varpi, \quad (1)$$

where  $\lambda_J$  is the mean longitude of Jupiter's orbit,  $\lambda$  is the asteroid's mean longitude and  $\varpi$  is the asteroid's longitude of pericentre.

The easiest surrogate to this problem is to define intersections of trajectories with some suitably defined plane (Roig et al. 2002) and record the values of orbital semimajor axis, eccentricity and inclination only here. These values are nearly fixed, apart from short-periodic variations, and may be called *pseudo-proper (resonant) elements*. Previous experience shows that a combined constraint

$$\sigma = 0 \wedge \frac{d\sigma}{dt} > 0 \wedge \varpi - \varpi_J = 0 \wedge \Omega - \Omega_J = 0 \quad (2)$$

is a good choice (here  $\varpi_J$  and  $\Omega_J$  are Jupiter's longitude of pericentre and longitude of node). When these conditions are satisfied, the semimajor axis  $a$  is minimum, the eccentricity  $e$  is maximum and the inclination  $I$  is maximum over a fairly long ( $\approx 10$  ky) interval of time.

In practice, however, short-period perturbations or secular-resonance effects make difficult to satisfy the above conditions exactly. A good operational compromise (e.g. Roig et al. 2002) is

$$|\sigma| < 5^\circ \wedge \frac{\Delta\sigma}{\Delta t} > 0 \wedge |\varpi - \varpi_J| < 5^\circ, \quad (3)$$

i.e., the condition for  $\sigma$  and  $\varpi - \varpi_J$  is satisfied only with a  $5^\circ$  precision and the time derivative of  $\sigma$  is substituted by the difference of  $\sigma$  in the two successive time steps.

Time series of the resulting pseudo-proper elements, hereafter denoted  $a_p$ ,  $e_p$  and  $I_p$ , are thus not technically constant but their variations are very small for stable orbits. Conversely, large variations of the pseudo-proper elements indicate orbit instability. We thus record pseudo-proper elements once per  $\approx 10$  ky, which is the characteristic circulation period of  $\varpi - \varpi_J$ . From these data, we compute the standard deviations,  $\sigma_a$ ,  $\sigma_e$  and  $\sigma_I$  over 1 My (see Table 1).

To make our work efficient, we implemented an on-line procedure for the pseudo-proper element computation and the second-order symplectic integrator<sup>2</sup> by Laskar & Robutel (2001) in the framework of the SWIFT package (Levison & Duncan 1994). The numerical simulations include gravitational perturbations by 4 giant planets and, when necessary (Sec. 3.1), Yarkovsky thermal forces. Perturbations by the terrestrial planets are neglected, except for a barycentric correction which we applied to the initial conditions of both massive planets and massless bodies. This approximation is reasonable for small eccentricity orbits in the outer part of the asteroid belt. The terrestrial planets are of minor importance even for high-eccentricity resonant orbits that cross their paths because the removal from the J2/1 resonance mostly happens when bodies have close encounters with Jupiter (e.g. Gladman et al. 1997). The terrestrial planets become more important when discussing whether Jupiter family comets or NEAs provide some objects to the J2/1 (Sec. 3.3), however, a full description of this issue is beyond the scope of this paper.

<sup>2</sup> The code, its documentation and a former poster presentation at the Asteroids, Comets and Meteors 2002 conference are publicly available at the web-site <http://sirrah.troja.mff.cuni.cz/yarko-site/>. We present tests of numerical integration accuracy, particularly in regards to how it depends on the selected time-step. This led us to the optimum time-step value used in this work.

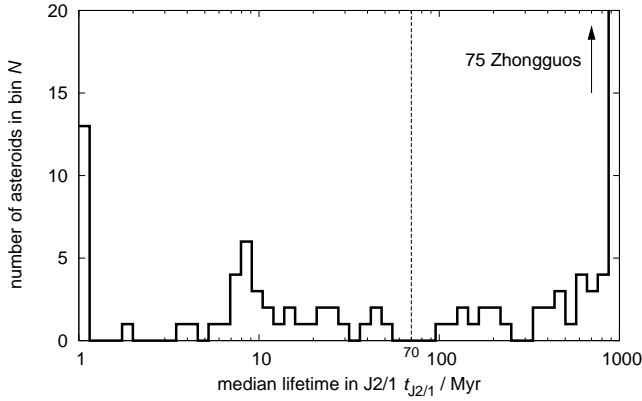


**Figure 1.** The distribution of the residence lifetime  $t_{J2/1}$  for the 153 asteroids inside the 2/1 mean motion resonance with Jupiter; note the log-scale on the abscissa. The unstable asteroids (i.e., those with  $t_{J2/1} \leq 70$  My) are separated from the long-lived asteroids by a dotted line. The first set includes two groups, one with extremely unstable asteroids ( $t_{J2/1} \leq 2$  My) in the first bin and another with relatively longer lifetimes ( $t_{J2/1} > 2$  My). The Griquas (i.e., dynamical lifetime greater than 70 My but shorter than the time-span of our 1 Gy integration) do not seem separated from the Zhongguos (with  $t_{J2/1} > 1$  Gy).

## 2.2 Resonant population

To properly characterize the J2/1 asteroid population, we proceed in two steps:

- (i) We integrate a large number of multi-opposition asteroids located near the J2/1 for 10 ky to identify those residing in the resonance;
- (ii) We track the orbital evolution of the identified resonant asteroids for 1 Gy, with the goal being to place them in one of the three resonant groups mentioned above.

Numerical simulations discussed in this section do not include Yarkovsky thermal forces. Initial orbital data for the asteroids were taken from the AstOrb (<ftp.lowell.edu>) database as of May 2004, while the initial orbital data and masses for the planets were from the JPL DE405 ephemeris. We only used numbered and multi-opposition asteroids in order to eliminate poorly constrained orbits. To select the initial sample of asteroids, we used the same criterion as Roig et al. (2002; Fig. 1), namely we considered asteroids whose osculating orbital elements are located in some broad region near the J2/1. With that procedure, we obtained  $\approx 4200$  asteroids whose orbits were propagated forward for 10 ky. We note the second-order symplectic integrator allows a longer time-step, 91.3125 days in our case, which speeds up the computation.

We output time series of the resonance critical angle  $\sigma$  for each asteroid. The orbits, characterized by the libration of  $\sigma$  and the osculating semimajor axes oscillating about an approximate centre at  $\simeq 3.276$  AU, reside inside the J2/1. We find 153 such cases,<sup>3</sup> including all asteroids found by

<sup>3</sup> We also found additional 9 asteroids for which the critical angle alternates between periods of circulation and libration in our 10 ky integration; these bodies are probably at the edge of the J2/1. There are also large families of non-resonant orbits, which exhibit libration of  $\sigma$ , but they circulate about the pericentric and

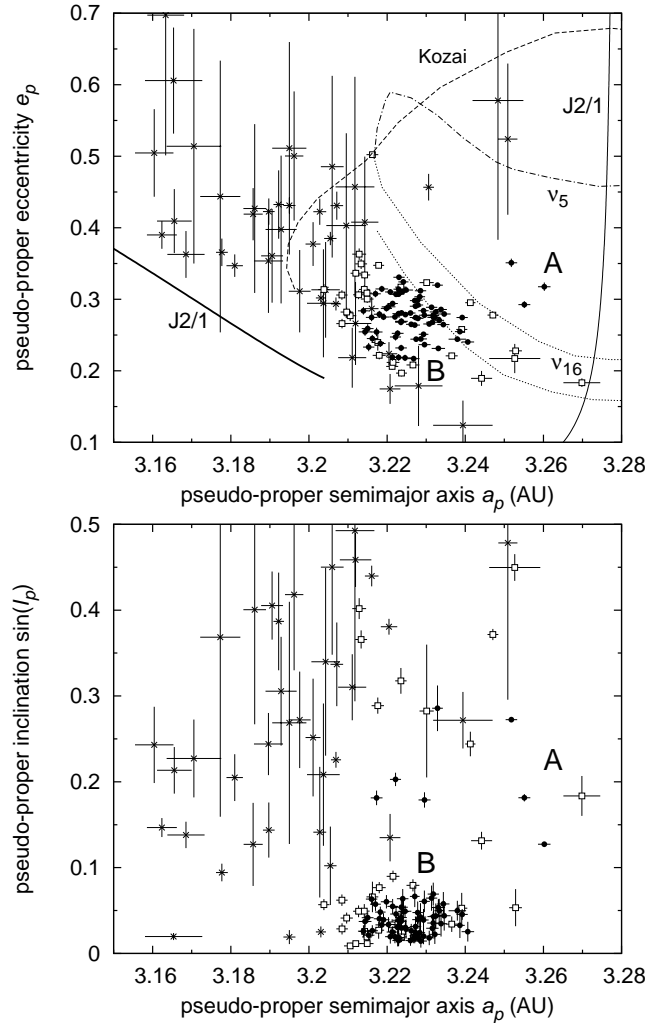


**Figure 2.** Pseudo-proper orbital elements of the asteroids residing in the J2/1 – semimajor axis  $a_p$  vs. eccentricity  $e_p$  (top), semimajor axis  $a_p$  vs. inclination  $\sin I_p$  (bottom). Bodies of different populations are indicated by different symbols: (i) the stable Zhongguos by full circles, (ii) the marginally stable Griquas by open squares, and (iii) the unstable asteroids by crosses. The error bars depict standard deviations of the pseudo-proper elements computed from a 1 My interval of time. The thin solid line labelled J2/1 is the libration centre (the pericentric branch) and the thick solid line J2/1 is the separatrix of the resonance (both shown for  $I = 0^\circ$ ). The dashed and dashed-dotted lines indicate borders of the most important secular resonances embedded inside the J2/1 (all shown for  $I = 10^\circ$ ; adapted from Moons et al. 1998), namely the  $\nu_{16}$  resonance (short-dashed), the Kozai resonance (dashed) and the  $\nu_5$  resonance (dash-dotted). A majority of the stable asteroids is clustered in the island B, while a few of them (see Table 2) are located in the island A, characterized by a higher mean eccentricity and inclination. All unstable asteroids are located in the chaotic zone where various secular resonances overlap. Griquas are a border-line population mostly at the edge of the B-region. In fact, 2-D projections shown here always lack clarity in showing 3-D structures; for that reason we posted a 3-D animation of the resonance structure with positions of the embedded asteroids at our web-site <http://sirrah.troja.mff.cuni.cz/yarko-site/>.

**Table 1.** Numbered and multi-opposition asteroids (situation as of May 2004) residing in the in the 2/1 mean motion resonance with Jupiter: the unstable population with median residence lifetime  $t_{J2/1} \leq 70$  My in our numerical simulation. (The complete list including also Zhongguos and Griquas can be found at our web-site <http://sirrah.troja.mff.cuni.cz/yarko-site/>.)  $a_p$ ,  $e_p$  and  $I_p$  are pseudo-proper resonant elements, computed with the method recalled in Sec. 2.1, and  $\sigma_a$ ,  $\sigma_e$  and  $\sigma_I$  are their standard deviations computed over 1 My time interval.  $H$  is the absolute magnitude taken from the `Ast0rb` database. The term “NEA” indicates bodies that are currently near-Earth asteroids; some additional objects will become NEAs in the next  $\sim 10$ ky due to the resonant variations of orbital semimajor axis and eccentricity.

| No.   | Name            | $a_p$<br>[AU] | $e_p$ | $I_p$<br>[deg] | $\sigma_a$<br>[AU] | $\sigma_e$ | $\sigma_I$<br>[deg] | $t_{J2/1}$<br>[My] | $H$<br>[mag] | Remark |
|-------|-----------------|---------------|-------|----------------|--------------------|------------|---------------------|--------------------|--------------|--------|
| 1921  | Pala            | 3.193         | 0.398 | 17.791         | 0.004              | 0.103      | 3.63                | 6                  | 14.3         |        |
| 1922  | Zulu            | 3.231         | 0.457 | 33.672         | 0.001              | 0.019      | 3.03                | 8                  | 12.2         |        |
| 5201  | Ferraz-Mello    | 3.100         | 0.531 | 4.984          | —                  | —          | —                   | 0                  | 14.8         |        |
| 5370  | Taranis         | 3.212         | 0.457 | 29.510         | 0.005              | 0.154      | 11.47               | 7                  | 15.7         | NEA    |
| 8373  | Stephengould    | 3.248         | 0.578 | 30.923         | 0.007              | 0.195      | 11.64               | 7                  | 13.8         |        |
| 9767  | Midsomer Norton | 3.163         | 0.697 | 34.687         | 0.005              | 0.196      | 7.13                | 0                  | 16.4         |        |
| 23577 | 1995 DY8        | 3.203         | 0.302 | 1.435          | 0.001              | 0.008      | 0.37                | 28                 | 14.6         |        |
| 26166 | 1995 QN3        | 3.251         | 0.524 | 28.578         | 0.002              | 0.106      | 10.53               | 8                  | 17.3         | NEA    |
| 31339 | 1998 KY30       | 3.198         | 0.311 | 15.793         | 0.003              | 0.058      | 3.22                | 9                  | 13.5         |        |
| 37237 | 2000 WZ161      | 3.171         | 0.514 | 13.131         | 0.007              | 0.164      | 2.60                | 1                  | 13.6         |        |
| 55068 | 2001 QX83       | 3.211         | 0.218 | 18.071         | 0.004              | 0.042      | 2.20                | 15                 | 13.2         |        |
| 65541 | 9593 P-L        | 3.190         | 0.423 | 8.266          | 0.002              | 0.018      | 1.84                | 10                 | 14.2         |        |
| 82009 | 2000 RF68       | 3.220         | 0.224 | 22.374         | 0.002              | 0.016      | 0.53                | 25                 | 13.22        |        |
| 83943 | 2001 WK14       | 3.192         | 0.432 | 22.758         | 0.001              | 0.048      | 3.26                | 7                  | 13.40        |        |
| 86358 | 1999 XB143      | 3.186         | 0.419 | 7.300          | 0.002              | 0.036      | 2.77                | 8                  | 12.65        |        |
| 86367 | 1999 XY223      | 3.178         | 0.366 | 5.411          | 0.002              | 0.019      | 0.59                | 17                 | 14.65        |        |
|       | 1977 OX         | 3.177         | 0.444 | 21.623         | 0.005              | 0.190      | 12.08               | 1                  | 15.20        |        |
|       | 1994 JC         | 3.167         | 0.930 | 30.446         | —                  | —          | —                   | 0                  | 15.14        |        |
|       | 1997 WW         | 3.201         | 0.377 | 14.567         | 0.002              | 0.031      | 3.93                | 14                 | 16.47        |        |
|       | 1997 YM3        | 3.195         | 0.511 | 15.583         | 0.004              | 0.149      | 8.11                | 13                 | 16.95        | NEA    |
|       | 1999 RM19       | 3.160         | 0.505 | 14.064         | 0.005              | 0.061      | 2.55                | 0                  | 13.68        |        |
|       | 2000 DB62       | 3.221         | 0.175 | 7.752          | 0.003              | 0.021      | 1.58                | 21                 | 13.95        |        |
|       | 2000 EU170      | 3.204         | 0.294 | 12.022         | 0.004              | 0.076      | 4.76                | 11                 | 13.64        |        |
|       | 2000 FH13       | 3.239         | 0.124 | 15.768         | 0.008              | 0.034      | 1.89                | 39                 | 13.38        |        |
|       | 2000 JV60       | 3.181         | 0.347 | 11.824         | 0.002              | 0.016      | 1.56                | 4                  | 17.21        |        |
|       | 2000 WL10       | 3.142         | 0.633 | 27.852         | —                  | —          | —                   | 0                  | 17.99        | NEA    |
|       | 2001 FF185      | 3.195         | 0.431 | 1.094          | 0.002              | 0.011      | 0.47                | 51                 | 16.32        |        |
|       | 2001 KD50       | 3.216         | 0.287 | 26.087         | 0.002              | 0.016      | 0.69                | 45                 | 13.35        |        |
|       | 2001 RP53       | 3.212         | 0.266 | 27.293         | 0.004              | 0.058      | 1.78                | 10                 | 14.21        |        |
|       | 2001 TK15       | 3.207         | 0.294 | 13.039         | 0.001              | 0.009      | 0.53                | 43                 | 13.50        |        |
|       | 2001 VE         | 3.196         | 0.500 | 24.716         | 0.002              | 0.090      | 5.06                | 4                  | 15.05        |        |
|       | 2002 CP56       | 3.205         | 0.385 | 5.863          | 0.002              | 0.009      | 2.62                | 25                 | 15.00        |        |
|       | 2002 GQ1        | 3.207         | 0.431 | 19.687         | 0.002              | 0.020      | 2.80                | 21                 | 14.39        |        |
|       | 2002 JH36       | 3.190         | 0.354 | 14.123         | 0.004              | 0.073      | 2.07                | 12                 | 15.91        |        |
|       | 2002 LN53       | 3.204         | 0.313 | 19.867         | 0.004              | 0.067      | 6.28                | 9                  | 14.53        |        |
|       | 2002 RC20       | 3.155         | 0.449 | 7.480          | —                  | —          | —                   | 0                  | 15.95        |        |
|       | 2002 RB107      | 3.186         | 0.427 | 23.613         | 0.003              | 0.118      | 7.67                | 0                  | 14.09        |        |
|       | 2002 WL         | 3.210         | 0.403 | 31.064         | 0.005              | 0.129      | 7.32                | 9                  | 14.43        |        |
|       | 2003 GP45       | 3.169         | 0.363 | 7.937          | 0.005              | 0.033      | 0.88                | 0                  | 16.53        |        |
|       | 2003 HG38       | 3.162         | 0.390 | 8.435          | 0.004              | 0.019      | 0.64                | 0                  | 15.65        |        |
|       | 2003 NS8        | 3.191         | 0.361 | 23.914         | 0.003              | 0.066      | 2.27                | 2                  | 13.72        |        |
|       | 2003 QW42       | 3.165         | 0.606 | 1.127          | 0.007              | 0.074      | 0.24                | 9                  | 14.41        |        |
|       | 2003 UL12       | 3.214         | 0.408 | 41.632         | 0.003              | 0.092      | 4.21                | 1                  | 17.19        | NEA    |
|       | 2003 WB8        | 3.206         | 0.485 | 26.748         | 0.003              | 0.127      | 5.86                | 6                  | 13.98        |        |
|       | 2003 WO87       | 3.203         | 0.422 | 8.123          | 0.002              | 0.018      | 4.37                | 23                 | 14.43        |        |
|       | 2004 GT2        | 3.228         | 0.179 | 37.394         | 0.006              | 0.056      | 0.89                | 8                  | 14.42        |        |
|       | 3260 T-1        | 3.166         | 0.409 | 12.321         | 0.004              | 0.045      | 1.56                | 0                  | 15.11        |        |

Roig et al. (2002). We find additional 100 J2/1 objects, some

apocentric branches of periodic orbits (e.g. Lemaître & Henrard 1990; Morbidelli & Moons 1993). We consider neither of them in our analysis.

discovered after 2001 and others that are previously known objects with more accurate orbits.

As a second step, we integrated our J2/1 asteroids for 1 Gy, with the goal being to classify them into one of the three groups described by Roig et al. (2002). Because of the inherent chaoticity of resonant motion, finite orbit accuracy,

**Table 2.** Numbered and multi-opposition asteroids residing in the stable island A of the J2/1. The quantities are the same as in Table 1. The last column indicates, whether the asteroid is classified as a Zhongguo (Z) or Griqua-like (G). Asteroid (4177) Kohman is a border-line case (see the text for discussion).

| No.   | Name       | $a_p$<br>[AU] | $e_p$ | $I_p$<br>[deg] | $\sigma_a$<br>[AU] | $\sigma_e$ | $\sigma_I$<br>[deg] | $t_{J2/1}$<br>[My] | $H$<br>[mag] | Remark |
|-------|------------|---------------|-------|----------------|--------------------|------------|---------------------|--------------------|--------------|--------|
| 78801 | 2003 AK88  | 3.260         | 0.318 | 7.309          | 0.002              | 0.006      | 0.14                | 1000               | 15.2         | Z      |
|       | 1999 VU218 | 3.241         | 0.295 | 14.125         | 0.001              | 0.002      | 0.82                | 771                | 15.25        | G      |
|       | 2001 FY84  | 3.253         | 0.217 | 26.727         | 0.007              | 0.020      | 0.89                | 152                | 14.06        | G      |
|       | 2003 SA197 | 3.252         | 0.351 | 15.807         | 0.001              | 0.006      | 0.09                | 1000               | 14.63        | Z      |
|       | 2003 YN94  | 3.255         | 0.293 | 10.451         | 0.002              | 0.005      | 0.24                | 1000               | 15.20        | Z      |
|       | 2004 FG32  | 3.247         | 0.278 | 21.816         | 0.001              | 0.004      | 0.37                | 536                | 14.53        | G      |
| 4177  | Kohman     | 3.233         | 0.320 | 16.598         | 0.001              | 0.001      | 1.52                | 1000               | 12.7         | Z      |

roundoff errors etc., any single integrated orbit may not represent that body’s true future motion (especially on time-scales significantly longer than the Lyapunov time, which is of order 10 ky here). To account for this, we gave each body a multitude of orbits so near the nominal solution that they represent statistically equal realizations of the orbit. We call these fictitious bodies “close clones”. Unlike previous studies, we consider 12 close clones for each of the identified resonant asteroids, produced by changing the nominal value of the semimajor axis by multiples of  $10^{-9}$  AU and the eccentricity by multiples of  $10^{-9}$  (well inside  $1\sigma$  uncertainty interval, as resulted from the orbit determination procedure).

About half of the objects were eliminated before the end of integration (due to perihelion distances smaller than the solar radius or heliocentric distances larger than 100 AU). This indicates they belong to the unstable or marginally stable populations. The remaining half of the objects survived in our simulation for 1 Gy inside the J2/1, suggesting a low diffusion rate among the stable population. We combine results for the close clones with that of the nominal orbit and define the residence lifetime  $t_{J2/1}$  for an asteroid inside the 2/1 resonance as their median value. Figure 1 shows the distribution of the lifetime values  $t_{J2/1}$  for the entire population of 153 resonant asteroids. Hereafter, we use this distribution to define the various asteroidal groups:

- long-lived:  $t_{J2/1} > 70$  My,
  - stable (“Zhongguos”):  $t_{J2/1} > 1$  Gy,
  - marginally stable (“Griquas”):  $t_{J2/1} \in (70, 1000)$  My,
- short-lived (unstable):  $t_{J2/1} \leq 70$  My,
  - extremely unstable:  $t_{J2/1} \leq 2$  My.

The results for individual unstable asteroids are summarized in Table 1. The classification and properties of all resonant asteroids can be accessed at our web-site <http://sirrah.troja.mff.cuni.cz/yarko-site/>.

Figure 1 shows it is reasonable to divide the short-lived and long-lived populations with an approximate threshold at 70 My. Our data further indicate that the unstable population – 47 asteroids in total – may contain  $\approx 25\%$  of objects on extremely unstable orbits (with  $t_{J2/1} \leq 2$  My). These objects may be separate from the remaining asteroids in this group. In the past, asteroids with long-lived orbits were previously classified as either Griquas (marginally stable) and Zhongguos (stable). We find, however, that this division is somewhat arbitrary and depends on the integration time-

span and the exact definition of the lifetime.<sup>4</sup> Indeed, Fig. 1 suggests there is no significant separation of lifetime values of the stable and marginally stable orbits. The marginally stable population appears to be a short-lived “tail” that adheres to the stable population; out of the 106 long-lived orbits we find 75 have lifetimes longer than 1 Gy, thus considered “stable”. In fact, our analysis, based on the 1 Gy integration only, does not permit a fine characterization of the stable population (e.g. the distribution of  $t_{J2/1}$  beyond the 1 Gy threshold).

Figure 2 shows a projection of the pseudo-proper orbital elements of the resonant asteroids on to the  $(a_p, e_p)$  and  $(a_p, \sin I_p)$  planes. The most important result here is a confirmation of the population classification discussed above. Orbits found to be unstable are located in the phase space region right where a number of secular resonances (like  $\nu_{16}$ ,  $\nu_5$  or Kozai resonance) embedded in the J2/1 overlap with one another. Because this zone of overlap extends to high orbital eccentricity values, the chaos caused by these overlapping resonances produces strong instability. Five bodies within the unstable population are currently NEAs, and several more will become NEAs within the next period of their libration cycle. This indicates there is an open “communication” between the NEA zone and the J2/1. In Sec. 4, we consider the possibility that NEAs feed part of the unstable population inside the J2/1. Conversely, the long-lived orbits are located in a stable zone, predicted previously by numerical and analytical methods (e.g. Nesvorný & Ferraz-Mello 1997; Moons et al. 1998). The marginally stable orbits occupy borders of this zone, while the stable orbits are confined near its centre. This explains the close connection between the two groups.

The long-lived asteroids in our sample tend to populate the stable niche called island B (Nesvorný & Ferraz-Mello 1997; Moons et al. 1998). However, Brož et al. (2004) reported for the first time the presence of several asteroids

<sup>4</sup> As a result, a number of asteroids classified stable by Roig et al. (2002) using their 520 My integration are marginally stable in our simulation spanning 1 Gy. For example, (3789) Zhongguo itself appears to reside on a marginally stable orbit with a median lifetime of 943 My (see also Moons et al. (1998) who reported a similar result). Note that we define characteristic lifetime as a median of the individual values for 12 close clones and the nominal orbit, while the previous studies usually only considered the nominal orbit.

inside the twin niche of stability called island A (Fig. 2). We detect 6 asteroids inside the island A (Tab. 2), i.e., having higher eccentricities and inclinations than the separatrix of the  $\nu_{16}$  secular resonance. Three of them reside on the marginally stable orbits and another three on the stable orbits. One of the Zhongguos – asteroid (4177) Kohman – is a border-line case because the critical angle of the  $\nu_{16}$  secular resonance ( $\Omega - \Omega_S$ ) alternates between periods of circulation and libration. Except (4177) Kohman, all asteroids inside the stable island A are small, with sizes ranging from 5.5 to 7.5 km (if 0.05 albedo is assumed). Interestingly, all asteroids in the island A have orbits with high inclination. Their proximity to the  $\nu_{16}$  secular resonance may be the reason, but we did not investigate this possible link in detail.

Despite these new island A asteroids, we confirm previous results suggesting that the stable island A appears under-populated as compared to the stable island B (e.g. Nesvorný & Ferraz-Mello 1997; Moons et al. 1998). In addition, our work allows us to place a quantitative constraint on the ratio of the number of A-Zhongguos (excluding A-Griquas) and the number of B-Zhongguos:  $3/71 \sim 0.04$ , but this ratio may change substantially as new asteroids residing on the stable islands will be discovered. Anyway, future work aim at explaining the origin of the long-lived resonant population should meet this constraint.

Figure 3 shows cumulative distributions of the absolute magnitude  $H$  for the resonant groups (we use magnitudes from the `AstOrb` database). We approximate these distributions over  $H = 12 - 14$ , with a power law:  $N(<H) \propto 10^{\gamma H}$ . The indices  $\gamma$  (slopes), calculated for the resonant groups, have the following mean values: 0.69 (with the interval of variation (0.64, 0.79)) for long-lived asteroids, 0.91 (0.81, 1.01) for Zhongguos, 0.33 (0.28, 0.48) for Griquas, and 0.78 (0.68, 0.88) for unstable asteroids. If we discard extremely unstable asteroids (i.e. those with  $t_{J2/1} \leq 2$  My) from the unstable group, we obtain somewhat shallower size distribution with the power-law slope of 0.66 (and the variation (0.56, 0.76)). We give here realistic maximal errors that were obtained by the variation of the interval over which  $\gamma$  was fitted and by random removal of a single asteroid from the population. To convert  $\gamma$  into the slope of a cumulative power-law size distribution, we multiply it by  $-5$ , making their mean cumulative slopes:  $-3.5$  (with the variation  $(-4.0, -3.2)$ ),  $-4.6$   $(-5.1, -4.1)$ ,  $-1.7$   $(-2.5, -1.4)$ ,  $-3.9$   $(-4.4, -3.4)$ , and  $-3.3$   $(-3.8, -2.8)$  respectively. For reference, a Dohnanyi-like cumulative slope is  $-2.5$  (Dohnanyi 1969). The indices for Zhongguos, Griquas and unstable asteroids are significantly different from each other, but the results for Zhongguos and Griquas depend sensitively on the threshold chosen for the division of the long-lived asteroids (1 Gy in our case).<sup>5</sup> Moreover, the Griquas have an unusual distribution of  $H$  that becomes steeper between  $H = 14 - 15$ . Because the Zhongguos and Griquas are not easily separable from each other, these source of these differences is difficult to investigate.

<sup>5</sup> If we select a smaller dynamical lifetime threshold, the size distribution of the Zhongguos generally becomes shallower and that of the Griquas becomes steeper. For example, for 0.5 Gy  $\gamma_{\text{Zhongguos}} = 0.77$  and  $\gamma_{\text{Griquas}} = 0.45$ .

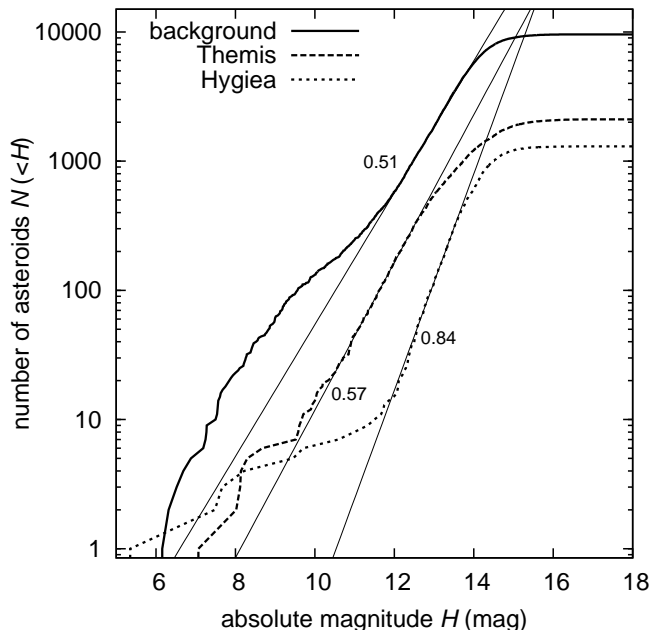


**Figure 4.** Cumulative distribution of the absolute magnitude for the three plausible source populations adhering to the J2/1 resonance: (i) the background asteroids (solid line), (ii) the Themis family (dashed line), (iii) the Hygiea family (dotted line). Lines are power-law approximations as in Fig. 3.

There are 16 asteroids with  $H \leq 14$  residing on unstable orbits. (This number is relevant for our analysis in Sec. 3.2.) Out of these 16 asteroids, 2 have extremely unstable orbits.

Except the problems with partitioning the long-lived population (which is not critical for this work), our results confirm those of Roig et al. (2002): at large sizes the resonant populations have a rather steep size distribution. Their slopes are steeper than a simple Dohnanyi-like collisionally evolved system would predict (Dohnanyi 1969), though this kind of system is unlikely to represent the main belt population except for bodies with  $D < 0.1$  km (e.g., Durda et al. 1998; O’Brien and Greenberg 2003; Bottke et al. 2004).

### 2.3 Source populations

An important conclusion follows from the comparison of the size distributions of the resonant groups and that of the plausible source populations: background asteroids, Themis family and Hygiea family. (These are the same populations as discussed later in Sec. 3.) Figure 4 shows the distribution of the absolute magnitudes for them, with the following fitted values of the power-indices: background  $0.51 \pm 0.01$ , Themis  $0.57 \pm 0.02$  and Hygiea  $0.84 \pm 0.02$ . We note the first two populations have distributions compatible with a Dohnanyi-like collisionally relaxed system for  $H \leq 12$  and  $H \leq 11$ , respectively (thus sizes approximately larger than 25 – 35 km). Hygiea’s distribution is considerably steeper at large sizes, but as shown by Morbidelli et al. (2003) it becomes significantly shallower at small sizes.

A significant difference in the exponent  $\gamma$  can be found between the source and resonant populations. The background asteroids differ from the unstable resonant asteroids

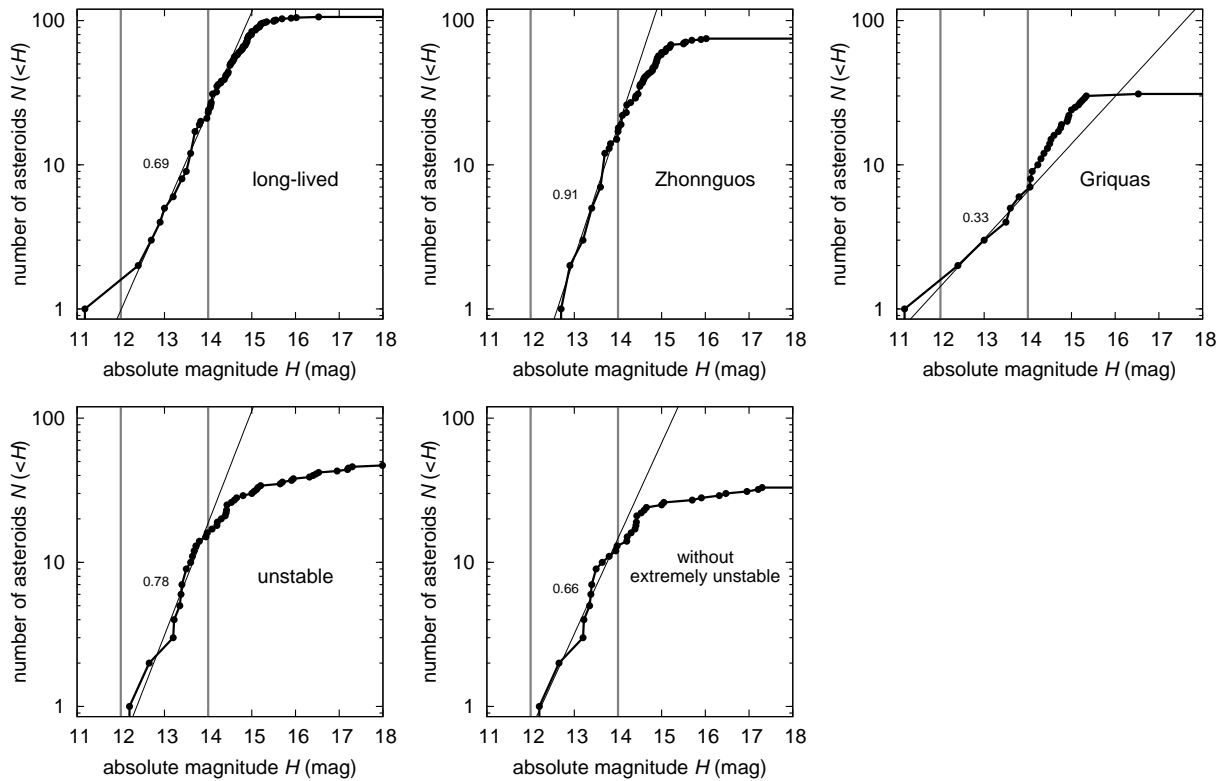


**Figure 3.** Cumulative distribution of the absolute magnitude for asteroidal populations inside the J2/1: (i) the long-lived asteroids together (top left), (ii) Zhongguos (top middle), (iii) Griquas (top right), (iv) the short-lived (unstable) asteroids (bottom left), and (v) the short-lived (unstable) asteroids with  $t_{J2/1} > 2$  My (i.e. extremely short-lived objects excluded; bottom right); note the semi-log axes. The straight lines indicate the best fit power-law approximations  $N(<H) \propto 10^{\gamma H}$  in the  $H$ -range of 12–14, delimited by vertical grey lines. The adjacent numerical labels are the resulting power-law indices  $\gamma$ . To convert  $\gamma$  into the slope of a power-law size distribution, we multiply by  $-5$ , making their cumulative slopes  $-3.5$ ,  $-4.6$ ,  $-1.7$ ,  $-3.9$ , and  $-3.3$  respectively. For reference, a Dohnanyi-like cumulative slope is  $-2.5$  (Dohnanyi 1969).

by  $\simeq 0.2 \pm 0.1$  (depending whether the extremely unstable asteroids are included in this comparison or not). A slope difference near 0.2 is compatible with the Yarkovsky-driven transport from the source region, because the Yarkovsky effect is size dependent (it scales as  $D^{-1}$  for “our” asteroids) and thus naturally causes this change of the source size distribution. On the other hand, the YORP effect, acting together with Yarkovsky, may cause the slope difference to decrease by  $\simeq 20\%$  (i.e. down to  $\simeq 0.15$ ; Morbidelli & Vokrouhlický 2003).

### 3 ORIGIN OF THE UNSTABLE RESONANT POPULATION

We now turn our attention to the origin of the unstable population. Our working hypothesis, motivated by similar studies of the NEAs and some of the weaker main-belt resonances, is that asteroids drifting in semimajor axis via Yarkovsky thermal forces should continuously resupply bodies to the J2/1 and keep the unstable population in an approximate steady state. For now, we assume that other sources, such as planet-crossing asteroids, Jupiter-family comets, collisional injection of material, and dynamical injections of bodies from weak resonances, provide only few bodies to the J2/1. We discuss this issue further in Sec. 3.3.

To test our hypothesis, we use both numerical and semi-analytical methods. Each has its strengths and weaknesses. For example, direct  $N$ -body simulations allow us to characterize the resonant dynamics, but computer time requirements do not allow us to track a statistically large sample of orbits. On the other hand, the semi-analytical approach foregoes any detailed description of a test body’s orbital evolution, but it does allow us to track a large enough sample of bodies that we can quantify results statistically while testing a wide range of model parameters. Our results for both approaches are described below.

#### 3.1 Numerical N-body model

Using a  $N$ -body model, our primary goals are to determine:

- (i) Residence time probability distributions (maps) indicating which portions of the orbital phase space are statistically most likely to be visited by test particles injected into J2/1 by Yarkovsky forces; and
- (ii) The characteristic lifetime test bodies spend inside the J2/1 before leaving it.

In a steady-state scenario, (i) can be directly compared with the orbital parameters of the observed asteroids, with a positive match supporting our model results. For (ii), the results, after some analysis and normalization, should be compara-



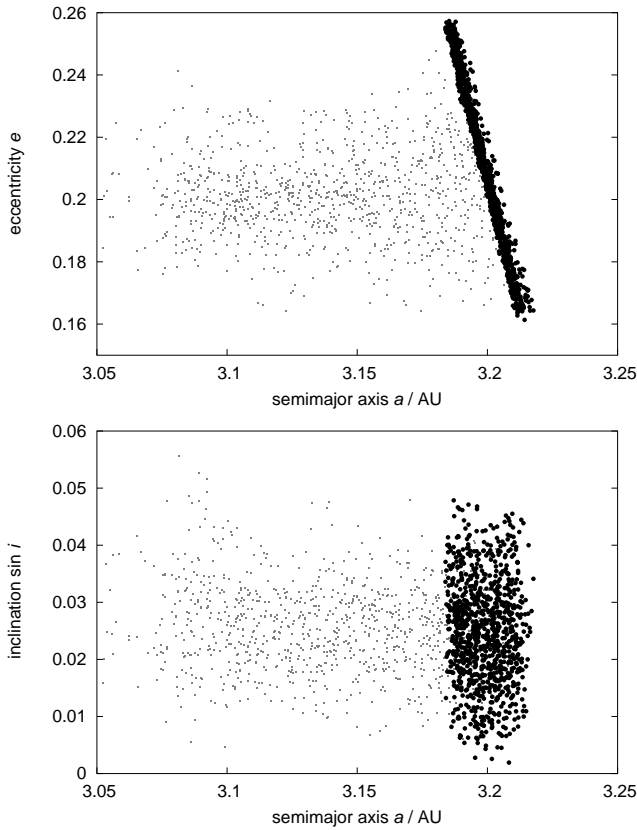


**Figure 5.** Initial orbital data for our numerical propagation of Themis family asteroids into the J2/1 resonance: pseudo-proper semimajor axis vs. eccentricity (top), semimajor axis vs. sine of inclination (bottom). The two groups of bodies are compared: (i) the Themis family members (gray dots), which were firstly identified in the proper element space at 70 m/s cutoff velocity (using data from *AstDyS* database) and then we calculated their pseudo-proper elements using the method described in Sec. 2.1; (ii) the test particles in our simulation (black circles). The initial osculating elements (not shown here) of the test particles are very close to the pseudo-proper ones, because of our choice of the initial longitude of pericentre. There is a large difference between the proper (non-resonant) and pseudo-proper (resonant) semimajor axis and eccentricity of the Themis family members; inclination is much less affected (this is because the fundamental resonant angle  $\sigma$  does not depend on the nodal longitude).

ble to the dynamical lifetime distribution obtained for the observed population in Fig. 1. This information is also used in the semi-analytical analysis described in Sec. 3.2.

Here we use the second-order symplectic integrator from Sec. 2 with Yarkovsky forces included. This is done by including Yarkovsky forces at the perturbation phase of the integrator. Test simulations verified analytical semimajor axis drift results for the thermal effects on asteroids on circular orbits. Both diurnal and seasonal variants of the thermal effects were included using a linearized approximation; the diurnal part is described in Vokrouhlický (1998, 1999) and the seasonal part is described in Appendix of Vokrouhlický & Farinella (1999). We use thermal parameters that are consistent with those expected for C-type asteroids: thermal conductivity  $K = 0.01$  W/m/K, specific thermal capacity  $C = 800$  J/kg/K, and surface and bulk densities

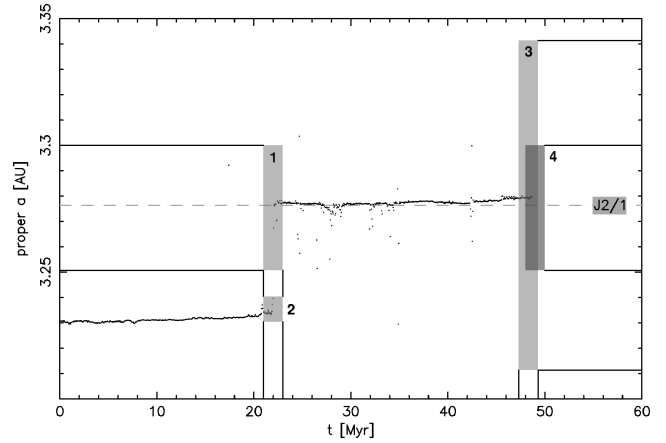


**Figure 7.** Mean semimajor axis  $a_m$  of the orbit from Fig. 6 as a function of time. Rectangles 1 to 4 represent diagnostic zones for the measurement of residence time in the J2/1. They move in time together with the orbital evolution, with rectangles 1, 3 and 4 staying centred at  $a_{J2/1} \simeq 3.2764$  AU. Here we designate the rectangles  $R_i$ , their widths  $t_I$ , and their heights  $a_i$  ( $i = 1, \dots, 4$ ). The operational condition for the entry time into the J2/1 is at least  $n_1$  data points are in  $R_1$  and the oscillations of  $a_m$  are smaller than  $R_2$ . A similar condition for their ejection time out of J2/1 is at least  $n_3$  data points are outside  $R_3$  or at most  $n_4$  data points are in  $R_4$ . In practice we use the following values:  $t_i = 2$  My ( $i = 1, \dots, 4$ ),  $a_1 = a_4 = 0.05$  AU,  $a_2 = 0.01$  AU,  $a_3 = 0.13$  AU,  $n_1 = n_3 = 50\%$ ,  $n_4 = 10\%$ .

$\rho_s = \rho_b = 1.5$  g/cm<sup>3</sup>. To let the bodies drift outward toward the J2/1, we set the initial obliquity to be 45°. We assumed rotation periods uniformly distributed in the range 4 – 12 h. Because Yarkovsky forces are size-dependent, we consider bodies with diameters in the range  $D = 4 - 40$  km. A combination of these parameters determines the magnitude and direction of the Yarkovsky perturbation and thus the orbital drift rate. However, our results only weakly depend on the strength of the Yarkovsky forces (see also Roig et al. 2002). The primary role of the Yarkovsky forces is to deliver the asteroids to the J2/1.

To test our hypotheses, we performed 3 simulations using 3 different source regions: (i) Themis family (using 1000 test particles with sizes from 4 to 40 km), (ii) Hygiea family, and (iii) the background main-belt population (both with 500 test particles with sizes from 16 to 40 km). The main difference between (i)-(iii) is the confinement of each source region's initial eccentricity and inclination values. The initial inclination of Themis and Hygiea family members are  $\simeq 1^\circ$  and  $\simeq 5^\circ$ , respectively. The orbital data of the background population, however, have inclinations over the interval  $\langle 0^\circ, 18^\circ \rangle$ . As an example, Fig. 5 shows the initial conditions of our simulation for asteroids evolving from the Themis family. All our test particles are started outside the J2/1 (the critical angle  $\sigma$  initially circulates), though to save computer time, they are placed close to the resonance. To that end, we chose the initial longitude of perihelion equal to that of Jupiter; this implies their eccentricity is at the top of the perturbation cycle. We note the pseudo-proper elements of the integrated particles match those of the family. Typically it takes several My to tens of My for our particles to evolve into the resonance (e.g. Fig. 6).

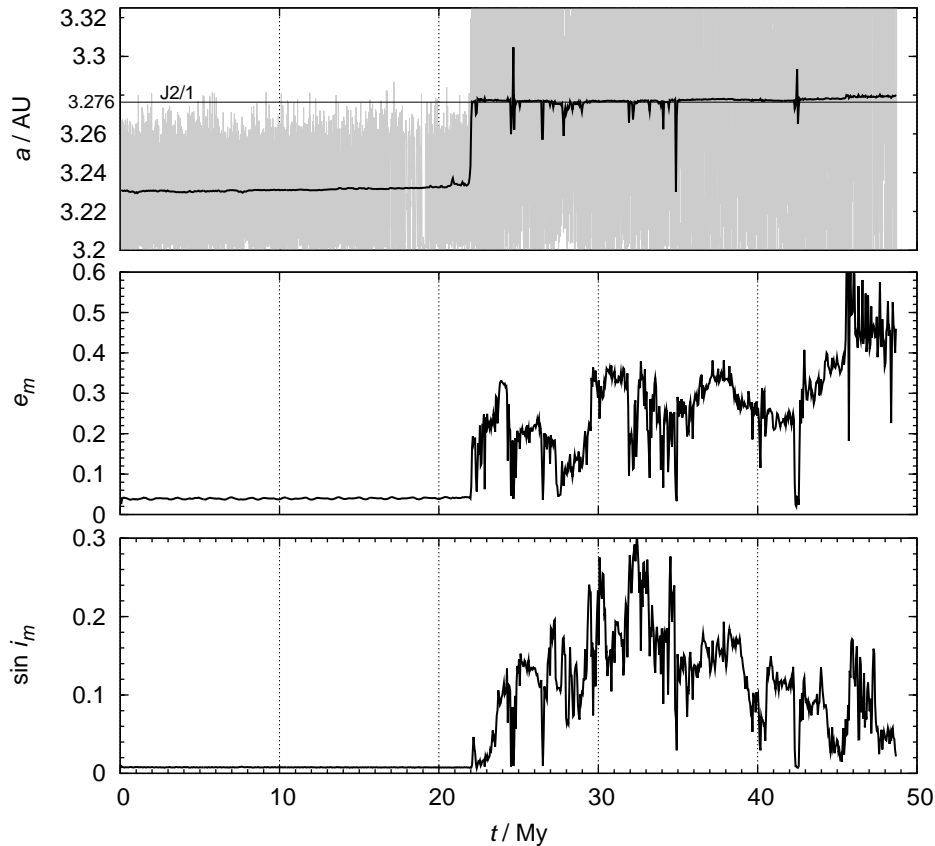


**Figure 6.** An example of a test body evolving into the J2/1 via Yarkovsky thermal forces; running-box mean orbital elements are shown as functions of time by bold black lines: semimajor axis  $a_m$  (top), eccentricity  $e_m$  (middle), and sine of inclination  $\sin i_m$  (bottom). The grey curve in the upper panel shows the osculating semimajor axis. At 22 My, the test body falls into the resonance, with the mean value of the semimajor axis “jumping” to  $\simeq 3.276$  AU (that of the stable periodic orbit in the resonance) while the osculating value starts to exhibit large oscillations. The eccentricity and inclination are pushed to high values, with their values affected by the  $\nu_5$  and  $\nu_{16}$  secular resonances embedded in the J2/1.

### 3.1.1 Example of an orbit evolving to the 2/1 resonance

Figure 6 shows a representative example of a test body evolving toward the J2/1 by the Yarkovsky effect. For analysis purposes, we compute mean values of the orbital elements –  $a_m, e_m, I_m$  – using on-line digital filters based on Kaiser window (Quinn et al. 1991) with an output time step 5 ky and further averaged over a running window 50 ky wide. Such “mean elements” do not have theoretical significance but they are useful auxiliary variables for our work.

We find the mean semimajor axis value  $a_m$  instantly jumps to  $\simeq 3.276$  AU upon entering the J2/1, with the osculating semimajor axis exhibiting large oscillations. This value corresponds to the J2/1 centre. Since the width of the J2/1 in semimajor axis is large, tracking the  $a_m$  time series allows us to easily determine when the orbit becomes trapped in the resonance (Fig. 7). A similar criterion applies to the instant the orbit leaves the resonance. For the latter, this mostly occurs when the J2/1 pushes the test body’s orbital eccentricity to a high enough value that it falls into the Sun or it is ejected from the inner Solar system as a consequence of a close encounter with Jupiter. We also computed the pseudo-proper orbital elements for each of the integrated orbits. These values were used to compare the evolutionary

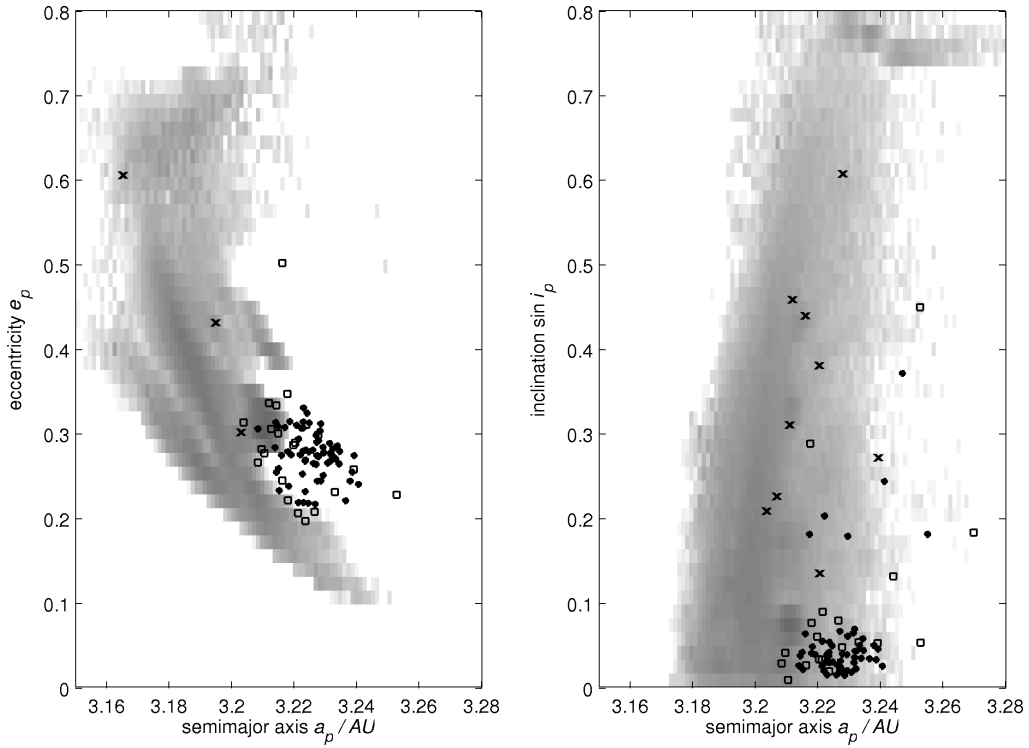
tracks of our test particles to observed asteroids located inside the J2/1 (Fig. 2).

In the next sections we separately analyse results for test bodies started in the Themis, Hygiea and the background populations.

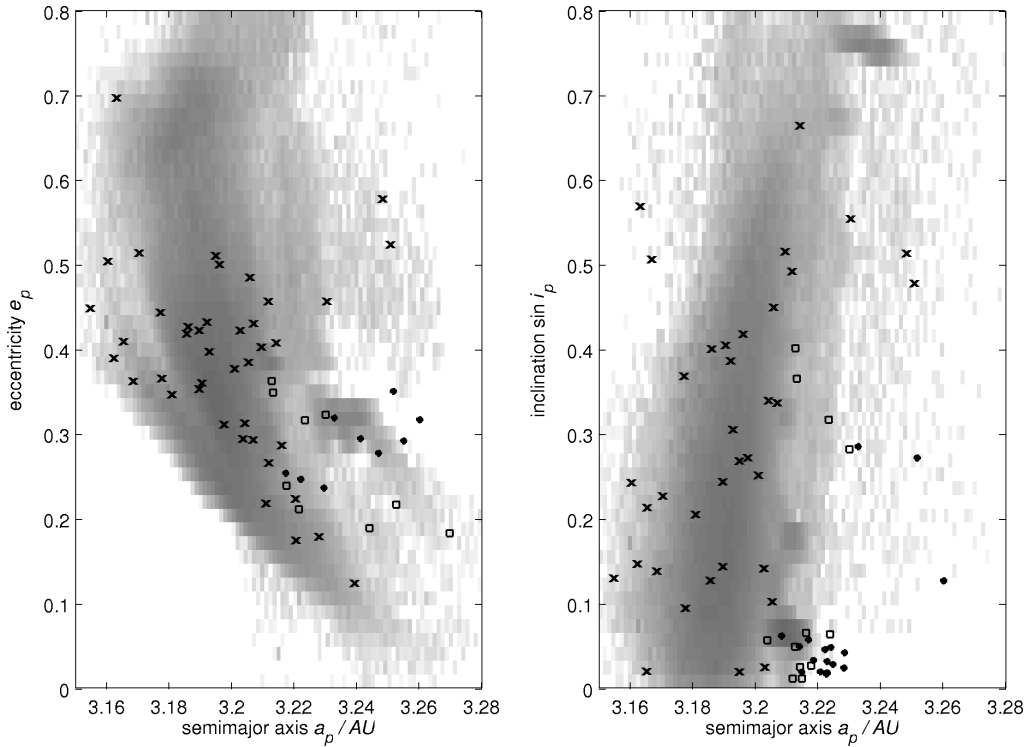
### 3.1.2 Themis family asteroids

To determine whether test bodies entering the J2/1 match with the location of asteroids inside the resonance, we need to define a quantitative measure of their residence. To do that, we assume there is a steady-state flow of asteroids into the J2/1 (see Sec. 1). Thus, any particle removed from the J2/1 is replaced by another from the source region. Assuming our sample of integrated orbits is representative, we track the amount of time spent by these test bodies in different regions of the J2/1. The cumulative time distribution produced by this procedure is believed to represent the true steady-state population inside the resonance (see Bottke et al. 2000, 2002 for similar ideas on populating the near-Earth asteroid orbits).

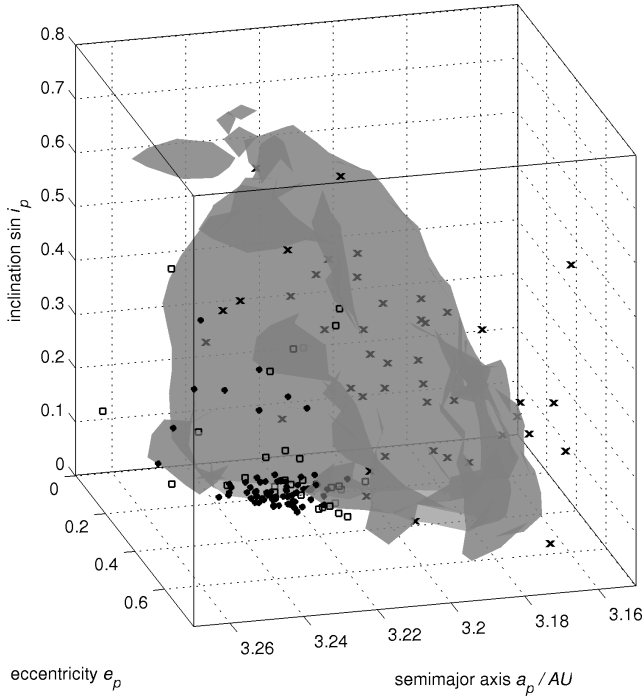
We construct a local number density  $n_{TP}$  of the test particles by summing the number of particles residing in the cell of the volume  $(\Delta a_p, \Delta e_p, \Delta \sin I_p)$  around the point



**Figure 9.** Two-dimensional projections  $Q_{\text{TP}}$  of the density particle function  $n_{\text{TP}}$  on to (i)  $(a_p, e_p)$  axes (with the restriction of  $I_p \leq 5^\circ$ ; left panel), and  $(a_p, \sin I_p)$  axes (with the restriction of  $e_p \leq 0.3$ ; right panel). The scale of grey indicates  $Q_{\text{TP}}$  in a logarithmic measure (blank for  $Q_{\text{TP}} = 0$  and the darkest for the maximum  $Q_{\text{TP}}$ ). Symbols denote positions of the observed populations inside the J2/1: (i) Zhongguos (filled circles), (ii) Griquas (squares), and (iii) the unstable asteroids (crosses).



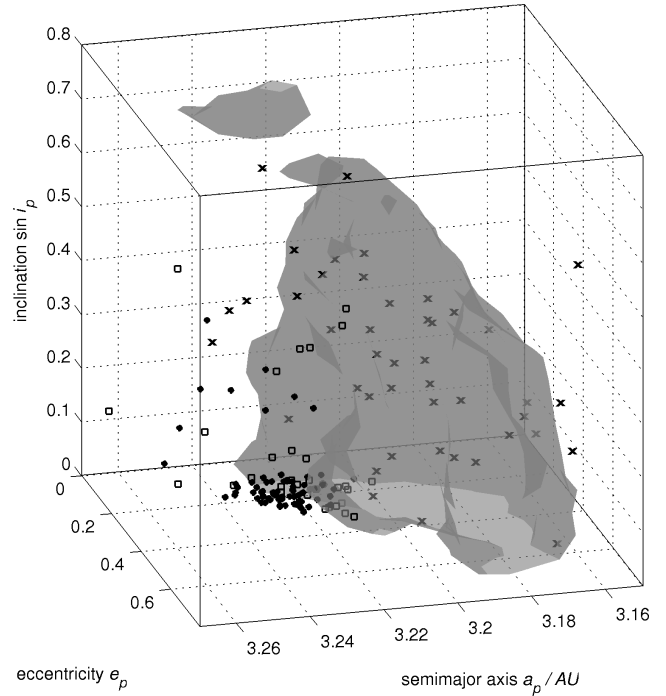
**Figure 10.** The same as in Fig. 9 but now data in the  $(a_p, e_p)$  projection show orbits with  $I_p \geq 5^\circ$  (left panel), and the  $(a_p, \sin I_p)$  projection show orbits with  $e_p \geq 0.3$  (right panel). Symbols as in Fig. 9.



**Figure 8.** An  $n_{TP} = 500$  iso-surface of the number density in the pseudo-proper orbital element space, resulting from our numerical simulation of test particles originating from the Themis family;  $n_{TP}$  reaches its maximum value of  $\simeq 3 \times 10^4$  inside this zone. Symbols denote positions of the observed populations inside the 2/1 resonance: (i) Zhongguos (filled circles), (ii) Griquas (squares), and (iii) the unstable asteroids (crosses). The 3-D surface is plotted as semi-transparent and one can distinguish the objects, which are in front of, inside or behind the surface, because they are gradually more and more gray/hidden. An illustrative animation with several coloured and partially transparent iso-surfaces can be found on <http://sirrah.troja.mff.cuni.cz/yarko-site/>.

$(a_p, e_p, \sin I_p)$  for *all* time steps during the *whole* span of our integration. Of course, values of the spatially dependent  $n_{TP}(a_p, e_p, \sin I_p)$  scale in some simple way with the volume of the cells, the time step  $\Delta t$  of the proper elements sampling and the time span  $\Delta T$  of the integration. In our case, we have  $\Delta a_p = 0.0075$  AU,  $\Delta e_p = 0.0025$ ,  $\Delta \sin I_p = 0.04$ ,  $\Delta t = 0.01$  My, and  $\Delta T = 1$  Gy. If one test particle stays in one cell for the whole 1 Gy, it would cause  $n_{TP} = 10^5$ . Regions with high  $n_{TP}$  values are likely locations to find observed asteroids (provided our hypothesis is correct). Regions with  $n_{TP} = 0$  are never visited by any of our integrated test particles and observed asteroids found in those locations cannot be explained by the Yarkovsky-driven transport from the given source region. Below, we show that the observed unstable asteroids are located in the regions of high  $n_{TP}$ , but the Zhongguos and Griquas are not. For the purpose of two-dimensional projections, we also define a column number density  $Q_{TP}$  as a sum of  $n_{TP}$  over all cells in the given direction, e.g.  $Q_{TP}(a_p, e_p) = \sum_{\sin I_p} n_{TP}(a_p, e_p, \sin I_p)$ .

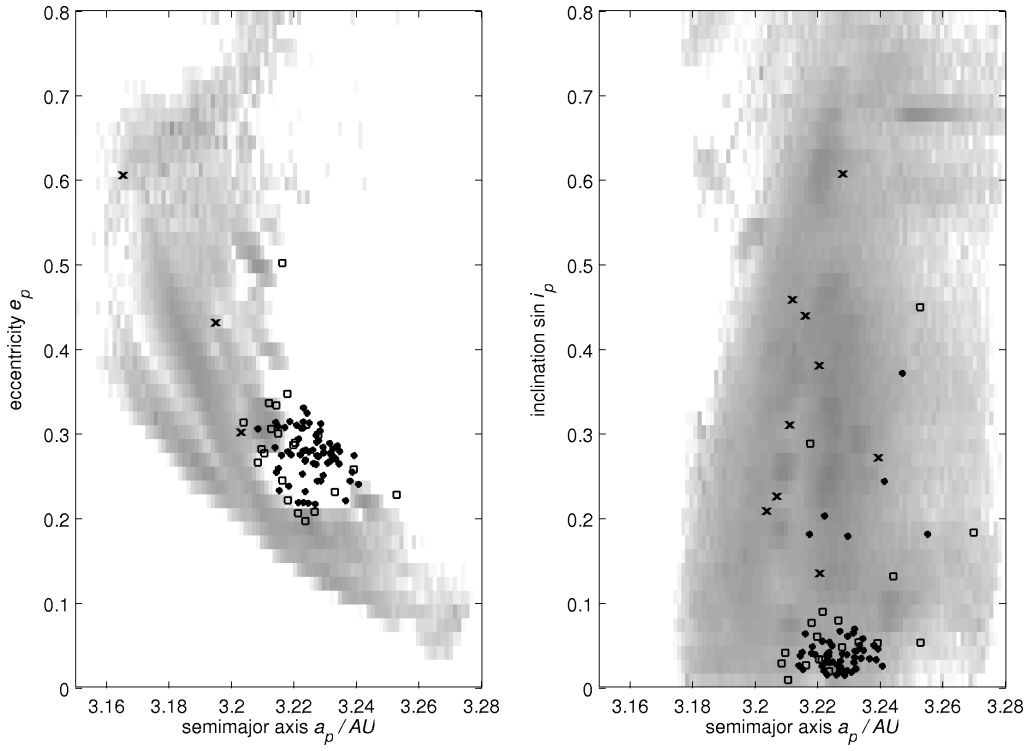
One difficulty in plotting our results is that the space of our pseudo-proper elements is in 3-D. This means that 2-D projections such as in Fig. 2 may result in misinterpretations. For that reason, we start with the complete 3-D representation and only with caution we use the 2-D maps.



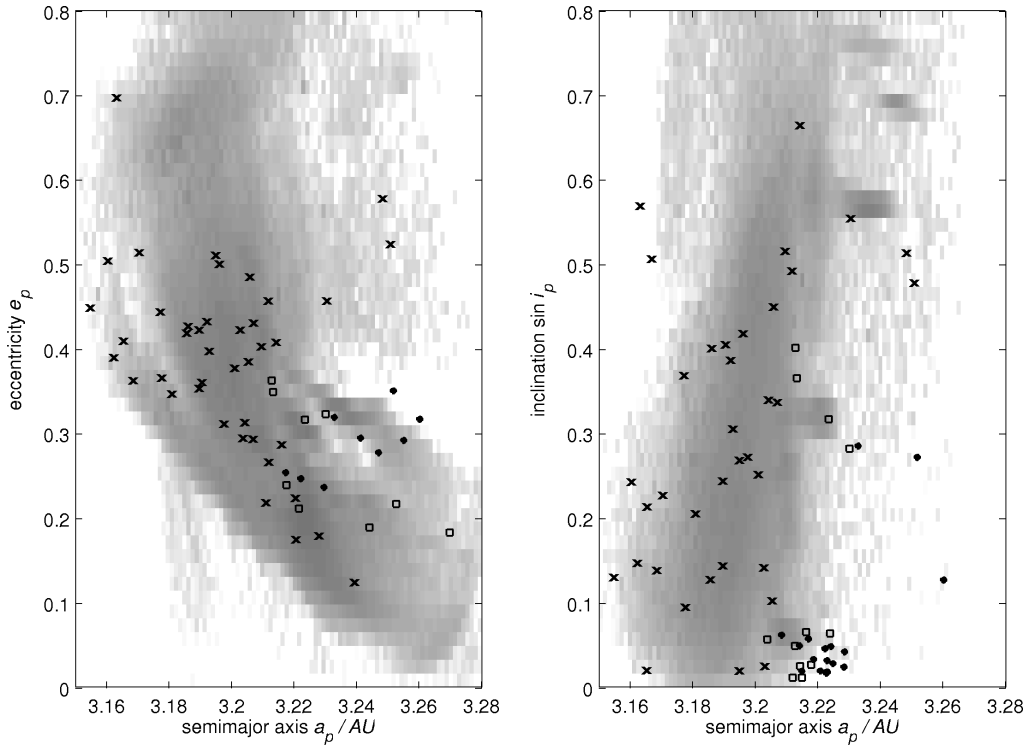
**Figure 11.** Here we show the same quantity as in Fig. 8 but now for the number density  $n_{TP}$  given as a weighted mean of the contributions by the three source populations: the background population (contributing by 84.5%), the Themis family (contributing by 14.2%) and the Hygiea family (contributing by 1.3%).

Figure 8 shows an iso-surface of moderately high value of the number density  $n_{TP} = 500$  in the space of pseudo-proper orbital elements. (its maximum value occurs inside the region). There is no important dependence of  $n_{TP}$  on size: bodies with size  $\geq 10$  km in our simulation yield the same result as those with size  $< 10$  km. Thus we present results for all particles together. Positions of the observed asteroids inside the J2/1 are shown by different symbols: Zhongguos (filled circles), Griquas (squares) and the unstable asteroids (crosses). Both long-lived populations (Zhongguos and Griquas) are situated outside the region of high  $n_{TP}$  values. The unstable asteroids, however, are located inside or close to the depicted iso-surface. This suggests their origin is compatible with our model of the Yarkovsky-driven transport into the J2/1.

Figure 9 shows 2-D projections of our previous results, where we focus on the long-lived asteroids. Note that their orbits tend to have low values of the pseudo-proper eccentricity and inclination. Thus, in plotting the  $(a_p, e_p)$  projection, we restrict ourselves to orbits with  $I_p \leq 5^\circ$  only (left panel), while in plotting the  $(a_p, \sin I_p)$  projection, we restrict ourselves to orbits with  $e_p \leq 0.3$  (right panel; see also Fig. 8 to get insight to the procedure). The value of the appropriate column number density  $Q_{TP}$  is given as the grey-scale colour. Our results confirm that the long-lived asteroids are mostly located in the blank regions where  $Q_{TP} = 0$ . Accordingly, their origin is incompatible with the delivery to the J2/1 by Yarkovsky forces. Note that while the 2-D representation suggests our integrated orbits populate the correct inclination values, this is not the case when the pseudo-



**Figure 12.** Here we show the same as in Fig. 9 but now for the column number density  $Q_{TP}$  given as a weighted mean of the contributions by the three source populations.



**Figure 13.** Here we show the same as in Fig. 10 but now for the column number density  $Q_{TP}$  given as a weighted mean of the contributions by the three source populations.

proper eccentricity is also taken into account (left panel and Fig. 8).

Figure 10 shows additional 2-D projections of our results, but now we focus on the unstable asteroids that typically have large eccentricity and/or inclination values (Table 1). Here we restrict to  $I_p \geq 5^\circ$  in the projection on the  $(a_p, e_p)$  plane (left panel) and to  $e_p \geq 0.3$  in the projection on to the  $(a_p, \sin I_p)$  plane (right panel). The orbits of the unstable asteroids, shown by crosses, match the zone of maximum  $Q_{\text{TP}}$  value (dark grey) in both projections. Only a few outliers can be found. This suggests our test bodies preferentially populate the resonant orbits occupied by the asteroids residing on the unstable orbits. In a few rare cases not shown here, we also observe test particles that jump across the J2/1 and populate the Cybele region (i.e., asteroids having  $a \in (3.3, 3.6)$  AU).

### 3.1.3 Hygiea family and background asteroids

We repeat our analysis for the Hygiea family and the entire background asteroid population. We find our results are nearly identical to those given above, such that we only plot the composite  $n_{\text{TP}}$  values constructed as a weighted sums from the three source regions. The weights used are the source contribution to the resonant population of  $H \leq 14$  asteroids estimated by our semi-analytical Monte-Carlo model (Sec. 3.2): the background population contributes by 84.5%, Themis and Hygiea families by 14.2% and 1.3%, respectively.

Figures 11 to 13 show the same results as Figs. 8 to 10, but now the composite number density  $n_{\text{TP}}$  is given. These results confirm that our test particles, evolving by the Yarkovsky forces from the adjacent main belt population to the J2/1, visit cells where the unstable asteroids are located and shy away from regions where long-lived asteroids are found. We note that none of our source regions match the distribution of the unstable population better than any other. This suggests the inclination of asteroids driven into the J2/1 is quickly mixed upon entry into the resonance, such that we cannot use the unstable population's orbital elements to estimate the source of a given resonant asteroid.

Figure 14 shows the residence time distribution  $t_{\text{J2/1}}$  for our test particles (bold solid line). As above, this is a weighted mean of the results for the 3 different source regions (the background population, Themis and Hygiea families), but there is only minor statistical difference between them. For the same reason, we also combine results here for large ( $\geq 10$  km size) and small ( $< 10$  km size) bodies. No permanent captures in the J2/1 were found, and no object entered stable resonant islands (see, e.g., Figs. 11 and 12).

A comparison between our test body residence times and those of the observed unstable objects shows the same order of magnitude (Fig. 1 and the dashed curve in Fig. 14). If we do not take into account the extremely unstable J2/1 object (with  $t_{\text{J2/1}} \leq 2$  My), the median of  $t_{\text{J2/1}}$  is 10.3 My for the observed unstable population (with  $t_{\text{J2/1}} \in (2, 70)$  My), and 14.7 My for our test particles. To make a more detailed comparison, we would need to perform additional modelling, mainly because we do not know how much time each of the observed asteroids already spent in the resonance. (The difference between the medians of  $t_{\text{J2/1}}$  can be attributed to

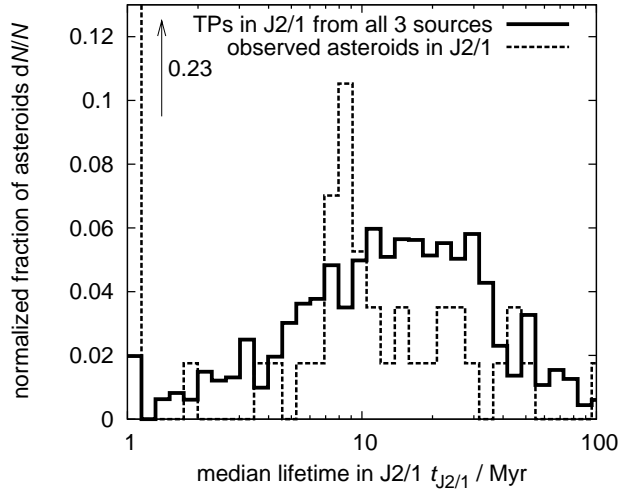


**Figure 14.** Distribution of the residence time inside the J2/1 for: (i) test bodies which were delivered into the J2/1 by the Yarkovsky effect (bold solid curve) and (ii) observed members of the unstable J2/1 population currently residing in the resonance (dashed curve; see also Fig. 1). In the case (i), the residence time records the time interval from entry into the J2/1 till escape out of the J2/1, while the case (ii) records the time interval from the present day to escape. The number of bodies  $dN$  in each logarithmic bin has been normalized by their total number  $N$ .

this effect.) However, the most important difference between the two plots is that our model does not predict the anomalously large number of extremely unstable J2/1 objects. We suspect some of these objects may be populated by other sources (Sec. 3.3).

## 3.2 Semi-analytical Monte-Carlo model

Next, we apply our semi-analytical model to the problem. Our primary goals are to determine, for a given source population adjacent to the J2/1:

- (i) The steady-state number of unstable asteroids inside the J2/1 with sizes larger than some threshold; and
- (ii) The slope of their size distribution.

We assume the steady-state situation for unstable J2/1 objects is valid and that the  $\approx 16$  unstable asteroids with  $H \leq 14$  are the steady-state number. We use the residence lifetimes of J2/1 test bodies estimated in the previous section. Given that Yarkovsky forces are size-dependent, we expect small asteroids will be delivered to the 2/1 resonance more efficiently than large ones. As a result, the size distribution of the target population should be different (steeper) than that of the source population. Figures 3 and 4 are consistent with this hypothesis, but we need to verify that the change of the power-law slope is what our model would predict.

### 3.2.1 Model setup

Our method is essentially the same as of Morbidelli & Vokrouhlický (2003). The first task is to characterize the source population for the J2/1. We then let the population

evolve into the J2/1 by Yarkovsky forces, where the semi-major axis drift speed depends on the spin-axis obliquity of each object. We assume that every asteroid removed from the J2/1 is replaced by a new object in the source population, which maintains a steady state. We neglect collisional disruption events since the dynamical lifetime for our bodies of interest in the J2/1 is short ( $\sim 10$  My) compared to their collisional disruption lifetime ( $\sim 1 - 2$  Gy for 10 km bodies; Bottke et al. 2004). Once the population in the J2/1 has reached the steady state, we compute the power-law slope of the resonant size distribution and compare it to observations (Fig. 3). Fluctuations in this population occur from time to time due to random injections of individual bodies (especially at large sizes). Our simulation is run for 4 Gy.

To construct the source region, we use the AstDyS (<http://newton.dm.unipi.it>) database, which includes all numbered and multi-opposition asteroids for which proper orbital elements have been computed. Somewhat arbitrarily, we use all asteroids that have proper semimajor axis  $a > 3.1$  AU and are located below the border of the J2/1. The J2/1 border is approximated in the proper semimajor axis  $a$  – proper eccentricity  $e$  plane by

$$e = c_0 + c_1 a, \quad (4)$$

where  $c_0 \simeq 10.82$  and  $c_1 \simeq -3.32 \text{ AU}^{-1}$ . Tests show that our results are not sensitive to these limits.

To compare our results with those in Sec. 3.1, we again split the population into 3 groups (i.e., Themis, Hygiea, and the background population). In Sec. 2, we characterized each in terms of their absolute magnitude  $H$  distribution (Fig. 4), but here we need to convert  $H$  into diameter  $D$  to obtain the correct strength of the Yarkovsky effect for each body.

The  $H$ – $D$  relationship depends on *a priori* unknown value of the geometric albedo  $p_V$  for each test asteroid. For this reason, we used two approaches: (i) we assumed a constant value  $p_V = 0.05$  appropriate for C-type asteroids, and (ii) we characterized  $p_V$  by a distribution function spanning some finite interval of values. For (ii), the albedo becomes a statistical quantity and thus our results become statistical properties requiring numerous simulations. The albedo distribution function maps on to parameters such as the estimated number of  $H \leq 14$  unstable asteroids residing inside the J2/1 resonance.

To determine appropriate albedo distribution for our model, we use values derived by Tedesco et al. (2002) from IRAS infrared observations. Unfortunately, the only resonant asteroid listed in this catalogue is (1362) Griqua. For this reason, we assume the albedo distribution of the resonant asteroids is similar to that of main belt asteroids in the neighbourhood of the J2/1. We thus select IRAS asteroids that fulfil the condition  $a > 3.1 \text{ AU} \wedge a < (3.260 + 0.301e) \text{ AU}$ , where  $a$  is the osculating semimajor axis and  $e$  the osculating eccentricity. The procedure yields 542 objects and a reasonably constrained albedo distribution (Fig. 15; we also verified that this distribution depends weakly on the orbit threshold chosen for the J2/1 border). Our albedo distribution peaks at 0.05, that same as assumed in (i), but there is a significant spread.

Figure 4 indicates the background population dominates the family contribution by a factor  $\simeq 5$  for  $H \leq 14$ –15, though we need to account for observational biases. To estimate the true background population, we extrapolated the

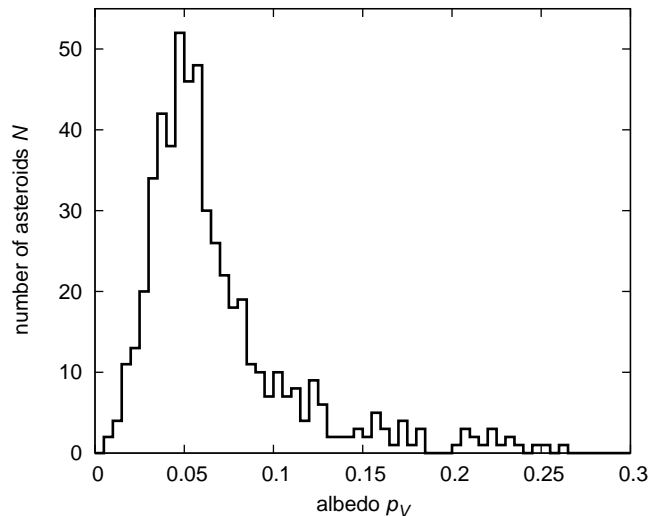


**Figure 15.** The distribution of albedo values derived by Tedesco et al. (2002) for asteroids located near the J2/1.

observed  $H$  distribution above the  $H \simeq 14$  threshold using the exponent  $\gamma \simeq 0.51$  (see Sec. 2.3). Using this procedure, we obtain a bias factor that is given by the ratio between the estimated and observed populations for different values of  $H$  for  $H > 14$ . The same factor is applied to the Themis and Hygiea families since they occupy roughly same main belt region. As described in Morbidelli et al. (2003), this procedure produces a bend in the slope of the family size distributions that is more shallow than the background main belt slope (this is especially remarkable for the Hygiea case, since it has a steep size distribution among its  $H < 14$  bodies). This simple debiasing procedure is acceptable for our purposes. Note that the  $H \leq 14$  source population is only increased  $\simeq 5\%$  relative to the observed sample. In our simulation, we consider asteroids down to  $H < 17.5$ , with the cumulative number being roughly half a million.<sup>6</sup>

Because our approach tracks individual test asteroids, every body has to have initial proper elements assigned to them. The observed asteroids are assigned their own orbital elements. The test asteroids obtain orbital elements of a randomly-chosen observed asteroid in the source population. This procedure somewhat neglects high inclination asteroids, which are harder to detect than low inclination asteroids, but this problem does not significantly affect our results.

We use a simplified orbital evolution model for our test asteroids that only accounts for changes in proper semimajor axis due to the Yarkovsky effect. We neglect the effects of weak mean motion resonances that force the population to diffuse in proper eccentricity and inclination (e.g. Nesvorný & Morbidelli 1998; Morbidelli & Nesvorný 1999). The proper semimajor axis of each asteroid changes according to:

$$\frac{da}{dt} = \kappa_1 \cos \epsilon + \kappa_2 \sin^2 \epsilon, \quad (5)$$

<sup>6</sup> Data on the faint asteroids, dominated by the inner main belt population, indicate the absolute magnitude distribution of the true population becomes shallower above a value of  $\simeq 15$  mag; e.g. Ivezić et al. (2001).

corresponding to the linearized analysis of the thermal effects (e.g. Vokrouhlický 1999). Here the first term is the contribution of the diurnal variant and second term is the contribution of the seasonal variant of the Yarkovsky effect. Both are dependant on the obliquity  $\epsilon$ . The diurnal case ( $\kappa_1$ ) is dependant on the rotation frequency  $\omega$ , while the seasonal case ( $\kappa_2$ ) is dependant on the mean orbital motion  $n$ . The dependence on thermal and bulk parameters, given in Sec. 3.1, is the same for both  $\kappa_1$  and  $\kappa_2$  functions. For our test asteroids, the diurnal Yarkovsky effect dominates, with  $\kappa_1$  larger by about an order of magnitude than  $\kappa_2$ . Hence, a test asteroid can migrate both inward or outward, depending on its obliquity  $\epsilon$ . For multi-kilometre bodies, both  $\kappa$ -functions are inversely proportional to the size of the body.

The orbital evolution of each asteroid is coupled to the evolution of its rotation frequency  $\omega$  and obliquity  $\epsilon$ . The evolution of these terms is complicated by torques from the variant of the Yarkovsky effect called Yarkovsky-Öpik-Radzievskii-Paddack (YORP) (e.g. Rubincam 2000; Vokrouhlický & Čapek 2002; Bottke et al. 2003; Vokrouhlický et al. 2003). Here we simplify YORP-driven dynamics to a steady variation of  $\omega$  and  $\epsilon$  as described by a system of two differential equations:

$$\frac{d\omega}{dt} = f(\epsilon), \quad (6)$$

$$\frac{d\epsilon}{dt} = \frac{g(\epsilon)}{\omega}, \quad (7)$$

where the functions  $f$  and  $g$  have been obtained by Čapek & Vokrouhlický (2004) for a large sample of objects with irregular shapes. Here we use their effective values obtained as medians over this sample. To recall a fundamental property of the YORP dynamics, we note it secularly drives the obliquity to some asymptotic values (for bodies with non-zero surface thermal conductivity the most likely values are  $0^\circ$  or  $180^\circ$ ), where the rotation speed is accelerated or decelerated with approximately the same probability (Čapek & Vokrouhlický 2004).

YORP evolution is expected to be temporarily halted by interactions with secular spin-orbit resonances. For low inclinations, it is a similar situation to Koronis prograde-rotating asteroids (Vokrouhlický et al. 2003). At sizes smaller than  $\simeq 10$  km, however, the YORP contribution might dominate. The evolution to asymptotic rotation states by YORP – very-fast or very-slow rotation rate – is still poorly understood, but the conventional wisdom is that (i) the acceleration of the rotation may result in mass loss and (ii) de-spinning triggers non-axial rotation or eventually drains so much rotational angular momentum from the body that collisions can re-orient and spin up the body. We use these assumptions in our simulation. We consider a given asteroid disrupted (and thus eliminated from our simulation) when its rotation period drops below 2 hr (see, e.g., Pravec et al. 2003). On the other hand, as the rotation period grows by YORP to a very large value (1000 hr in our simulations), we assume a collisional re-orientation event is likely to take place (see below).

The Yarkovsky and the YORP effects make our initial source population evolve smoothly toward the boundary of the J2/1 (Eq. (4)). Once the orbit crosses the resonance border, it is recorded as a resonant asteroid in our model. Numerical simulations from Sec. 3.1 suggest these test as-

teroids become members of the unstable population. We use these simulations to estimate the residence time of the objects in the J2/1 (Fig. 14). We assume the body is eliminated from the resonance after some period of time, with a new body injected into the source population to maintain the steady state. The output of our simulation is a time series of asteroid residence times inside the J2/1.

Finally, our simulation also includes a rough treatment of collisional disruptions. We assume these events occur with a time-scale  $\tau_{\text{disr}}$ . Additionally, because of the Yarkovsky effect dependence on the obliquity and the rotation frequency, we assume non-disruptive collisions can change asteroid's spin state with a time-scale  $\tau_{\text{reor}}$ . Following Farinella et al. (1998), with an update by Farinella & Vokrouhlický (1999), we have

$$\tau_{\text{disr}} = A (R/R_0)^\alpha, \quad (8)$$

$$\tau_{\text{reor}} = B (\omega/\omega_0)^{\beta_1} (R/R_0)^{\beta_2}. \quad (9)$$

The coefficients  $A$  and  $B$  in the equations are somewhat uncertain and depend on assumptions about the internal structure and physical processes associated with large asteroid disruptions and dispersal into fragments. Farinella et al. (1998) give: (i)  $A_{\text{nom}} = 16.8$  My and  $\alpha = 1/2$  for the collisional time-scale ( $R_0 = 1$  m is the reference value for the radius), and (ii)  $B_{\text{nom}} = 84.5$  ky,  $\beta_1 = 5/6$  and  $\beta_2 = 4/3$  for the reorientation time-scale (with the reference rotation frequency  $\omega_0$  corresponding to the rotation period of 5 hr). These estimates were obtained for a projectile population with the equilibrium exponent  $-2.5$  of the cumulative size distribution (different values of this parameter produce different values of the exponents  $\alpha$ ,  $\beta_1$  and  $\beta_2$ ).

The effective calibration of the time-scale, coefficients  $A$  and  $B$ , were obtained for the mean material parameters of silicate bodies and mean impact parameters in the main-belt. For this study, we note that  $A \propto S^{5/6}$  (Farinella et al. 1998), where  $S$  is the impact strength of a target. Since the prevalent C-type objects in the outer part of the main asteroid belt have a strength about an order of magnitude less than basaltic material (e.g. Davis et al. 1985; Marzari et al. 1995, Sec. 4.2), about an order of magnitude smaller value  $A \simeq 1.7$  My might be also possible. For that reason we introduce an empirical scaling parameter  $c_1$ , so that  $A = c_1 A_{\text{nom}}$  and  $c_1 \in \langle 0.1, 1 \rangle$ . Similarly, we introduce a scaling parameter  $c_2$ , so that  $B = c_2 B_{\text{nom}}$ , and  $c_2 \in \langle 0.1, 1 \rangle$ .

### 3.2.2 Results

Figures 16 and 17 summarize results of our nominal simulation, with  $A = A_{\text{nom}}$  and  $B = B_{\text{nom}}$  (thus  $c_1 = c_2 = 1$ ), and a geometric albedo  $p_V = 0.05$ . Figure 16 shows the size distribution of the resulting unstable population (solid lines). In order to characterize its power-law slope, we do not consider the population at any given time instant but instead we include all asteroids residing in the J2/1 resonance during a given interval of time (i.e., a running window of 2 Gy with initial epochs 0.5 Gy, 1 Gy, 1.5 Gy and 2 Gy, with the initial epoch excluded to let the system settle near steady-state equilibrium). Thus, in this plot, the absolute number



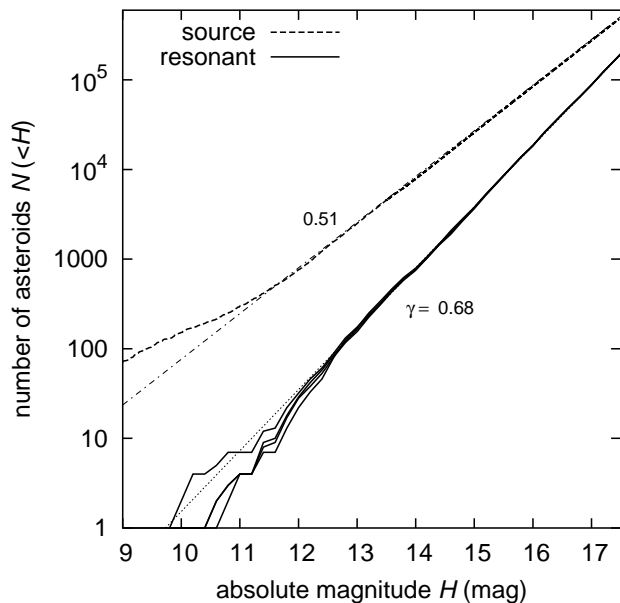


**Figure 16.** Cumulative  $H$  distribution of the simulated unstable population in the J2/1 (solid curves) compared with the source population (dashed curve). All 3 source populations are considered together. Large  $H$  values were found by extrapolating from small  $H$  values using a power law (compare the dashed curve with the dotted curve in Fig. 4). The 4 solid lines are distributions of resonant population collected during 2 Gy windows: 0.5 – 2.5 Gy, 1 – 3 Gy, 1.5 – 3.5 Gy and 2 – 4 Gy. They are nearly identical at small sizes but fluctuate at large sizes because some large asteroids occasionally fall in the resonance. Straight lines are local power-law approximations in the  $H$  range 12 – 14 (labels are the corresponding exponent value). Here we use our nominal model,  $A = A_{\text{nom}}$  and  $B = B_{\text{nom}}$ . All asteroids have the same albedo value  $p_V = 0.05$ .

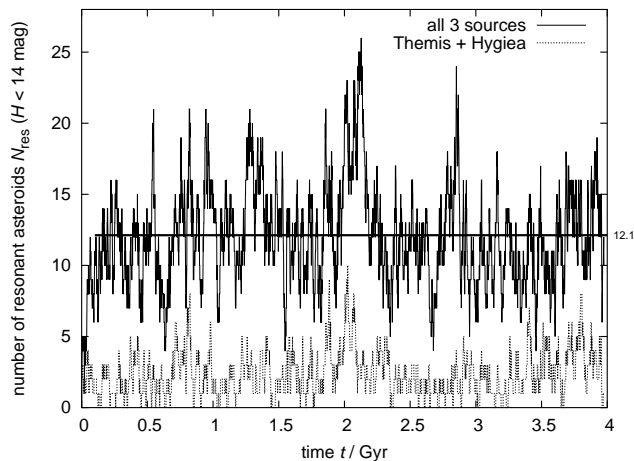


**Figure 17.** Estimated steady-state population of the unstable asteroids with  $H \leq 14$  inside the J2/1 in our nominal simulation where all asteroids are assumed to have  $p_V = 0.05$ . Fluctuations around the mean value of  $\simeq 12$  are due to random injections into the resonance. The bottom dotted curve shows the contribution of the Themis and Hygiea families,  $\simeq 15\%$  of the total.

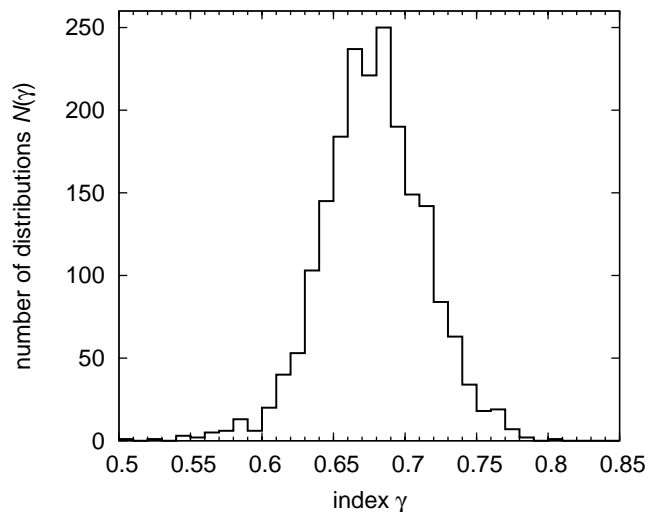


**Figure 18.** Distribution of the slope parameter  $\gamma$  fit to the simulated population inside the J2/1 on unstable orbits with  $12 < H < 14$ . Here we use nominal values of the collision and reorientation strength, thus  $A = A_{\text{nom}}$  and  $B = B_{\text{nom}}$ . We assume asteroid albedo has the same distribution seen in Fig. 15; we ran 50 simulations with different random seed to assign albedos/sizes to individual asteroids.

of J2/1 asteroids is not relevant.<sup>7</sup> The power-law index is found by fitting a line to the mean value of the fluctuating indices during the time window of 2 Gy. In spite of fluctuations produced by large asteroids, we note the distribution function of  $12 < H < 14$  is well characterized by a power-law index  $\simeq 0.68 \pm 0.05$  (the error bar is dominated by fluctuations over time). This agrees with the observed population (Figs. 3; recall that the observed slope of the  $H \leq 14$  asteroids on the unstable orbits becomes  $0.66 \pm 0.1$  when the extremely unstable orbits are excluded) and is significantly steeper than the slope of the main belt source population adjacent to the J2/1 ( $0.51 \pm 0.01$ ). This change in slope is produced by Yarkovsky and YORP forces (e.g. Morbidelli & Vokrouhlický 2003).

Figure 17 shows the simulated number of resonant asteroids with  $H \leq 14$  residing in the unstable population during the 4 Gy simulation. After a  $\simeq 0.1$  Gy transition phase, the system settles into fluctuations about the stationary value of  $\simeq 12$  asteroids. This number comes primarily from a combination of the available source population and strength of the Yarkovsky effect. This result agrees well with the observed 16 asteroids with  $H < 14$  on unstable orbits (Sec. 2). Note that fluctuations as high as 25 bodies are possible. It is also possible that several of the highly unstable bodies came from a different source (see Sec. 3.3).

Using our nominal parameters for collisional effects,

<sup>7</sup> We also occasionally obtain very large asteroids – up to 60 km size – injected into unstable population of the J2/1 resonance, but these events are very rare, about  $\simeq 0.5\%$  probability. This may be why we currently do not observe them. We obtained our probability estimate by comparing the typical residence lifetime –  $\simeq 10$  My (Fig. 14) – with the width of the sampling window (2 Gy). It is also possible that these large asteroids are missing in the resonant population because the assumption of their steady-state production in the source population is violated.

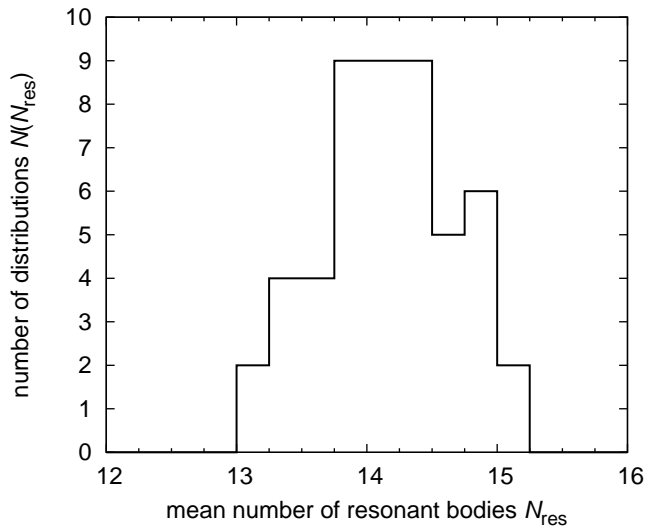


**Figure 19.** Distribution of the mean value for the number of asteroids with  $H \leq 14$  in the J2/1 on unstable orbits. See Fig. 18 for details.

$A = A_{\text{nom}}$  and  $B = B_{\text{nom}}$ , we tested how varying the albedo – approach (ii) above – would change our results. Using a different seed for our random-number generator, we created 50 possible source populations with different albedo values attributed to the individual asteroids and ran 50 simulations. Each time, we recorded the parameters shown in Figs. 16 and 17, namely the equilibrium number of asteroids with  $H \leq 14$  inside the J2/1 and the index  $\gamma$  of the cumulative  $H$ -distribution for  $12 < H < 14$ .

We find the mean value of the expected power-index  $\gamma$  of the resonant population is  $\simeq 0.68 \pm 0.05$  (Fig. 18). The expected steady-state number of resonant asteroids on unstable orbits is  $\simeq 14 \pm 1$ . This is a slight increase from our previous simulation because asteroids with higher albedo values have, for a given  $H$ , smaller  $D$  values and thus they drift faster via Yarkovsky forces. The albedo distribution shown in Fig. 15 is slightly asymmetric about the mean value 0.05, with a longer tail toward higher albedo values. On the other hand, the observed increase in the steady-state number of resonant asteroids is within the time fluctuations seen in Fig. 19.

We find the results of the nominal simulations do not change much with varying  $c_1$  and  $c_2$  (Fig. 20). For example, for the lowest values of  $c_1$  and  $c_2$ , the estimated equilibrium number of  $H \leq 14$  unstable resonant asteroids drops to  $\sim 9$ . This is because frequent collisions and spin axis re-orientations effectively weaken Yarkovsky delivery to the resonance. The work on collisional evolution of the main asteroid belt (Bottke et al. 2004), and hints from anomalous spin axes distribution of asteroids in the Koronis family (Vokrouhlický et al. 2003) suggest that the lowest  $c_1$  and  $c_2$  values are unlikely.

Similar values are found by weakening the YORP effect. For example, dropping the strength of YORP by an order of magnitude produces, with our nominal time-scales (i.e.  $c_1 = c_2 = 1$ ), some 10 unstable asteroids. Only removing the YORP effect entirely from our simulation produces a smaller number –  $\simeq 5$  – of large unstable asteroids. This shows how the YORP effect helps deliver asteroids into the

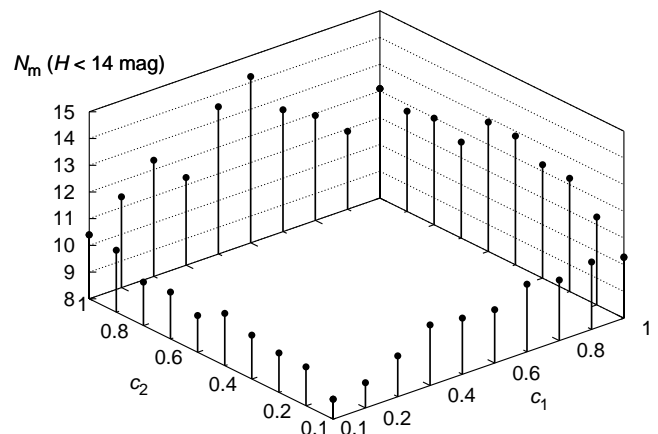


**Figure 20.** The estimated equilibrium number of  $H \leq 14$  asteroids residing on unstable resonant orbits as a function of  $c_1$  and  $c_2$  (i.e. modifications of the collisional lifetime –  $c_1$  – and spin-axis reorientation time-scale –  $c_2$ ; the nominal result from Fig. 17 corresponds to  $c_1 = c_2 = 1$ ). All bodies have fixed albedo  $p_V = 0.05$ .

J2/1: by preferentially tilting obliquity toward extreme values, YORP increases Yarkovsky drift.

### 3.3 Very unstable objects in the J2/1 resonance

As described previously, the J2/1 objects with very short dynamical lifetimes ( $\leq 2$  My; Fig. 1) do not appear to come from the asteroid populations located along the J2/1 periphery. Instead, we explore in this section whether these very unstable objects are Jupiter family comets (JFCs) or near-Earth asteroids (NEAs) that have become temporarily captured inside the J2/1. Note that such trapping behaviour near separatrix of resonant zones has been observed in many different numerical simulations (e.g. Levison & Duncan 1994; Malyskin & Tremaine 1999; Efthymiopoulos et al. 1999; Levison & Duncan 1997; Bottke et al. 2000, 2002).

To test our hypothesis, we turn to the results of Bottke et al. (2002), who tracked test bodies from numerous near-Earth object (NEO) sources in order to model the orbital  $(a, e, i)$  distribution of the NEO population. As part of their model, Bottke et al. (2002) numerically integrated test bodies from their source regions until they struck a planet, the Sun, or were ejected via a close encounter with Jupiter. Using results from their modelling work, we find that the objects most likely to become temporarily trapped in the J2/1 are active and dormant comets from the transneptunian disk (see also Levison & Duncan 1997, whose numerical integration runs are used in Bottke et al. 2002). We use these results to quantify the number of test bodies in the J2/1.

Bottke et al. (2002) estimated approximately  $(6 \pm 4)\%$  of all NEOs with  $a < 7.4$  AU are dormant JFCs. If there are a steady-state number of  $\simeq 1100$  NEOs with  $H < 18$ , this works out to be roughly 20 – 110  $H < 18$  NEOs from the dormant JFC population. Using the Bottke et al. (2002) residence time probability distribution computed for Jupiter-family comets, we estimated the number of dormant comets in the J2/1 at any given time. Our residence time distribution was normalized to those objects reaching

perihelion  $q < 1.3$  AU and  $a < 7.4$  AU. We found that the fraction of comets trapped in the J2/1 resonance (i.e.,  $3.2 \text{ AU} \leq a \leq 3.4 \text{ AU}$  and  $q > 1.3 \text{ AU}$ ) is  $\simeq 9\%$  of the JFC/NEO population. Thus, this implies that the dormant comet population in the J2/1 is 2–10 objects with  $H < 18$ .

To include active comets, we turn to results described in Levison et al. (2002), who estimated that the ratio of dormant comets with  $H < 18$  to active comets in the JFC population is roughly 2. Using this ratio, we expect the number of active comets in the J2/1 should be 1–5. The upper limit is consistent with the observed number of  $\simeq 5$  active comets currently trapped in the J2/1 (i.e., 83P/Russell 1, 104P/Kowal 2, 124P/Mrkos, P/LINEAR (2000 B3) and P/LINEAR (2000 R2)). Note that these bodies were identified by numerical integrating comets (without non-gravitational forces) using the orbital elements contained in the Jet Propulsion Laboratory database [http://ssd.jpl.nasa.gov/sb\\_elem.html](http://ssd.jpl.nasa.gov/sb_elem.html). Our results indicate these comets typically remain trapped in the J2/1 for tens to hundreds of ky, consistent with the dynamical lifetimes of the very unstable objects.

Our results imply the upper limit of the  $H < 18$  dormant comet population described above (10 objects) is the most applicable to our estimates. We caution, however, that active JFCs with  $q < 1.3$  AU pass closer to the Sun than those with  $q > 1.3$  AU and thus may be more prone to thermal-driven splitting and disruption events. Because results from Bottke et al. (2002) have only been calibrated for bodies with  $q < 1.3$  AU, we may be somewhat underestimating the number of dormant comets in the J2/1.

Levison et al. (2002) claim that dormant comets are likely to follow a cumulative  $H$  distribution with a power-law index of  $\gamma = 0.23 - 0.28$ , where  $N(< H) \propto 10^{\gamma H}$ . Using the values above, this suggests that  $\simeq 1$  dormant comet with  $H < 14$  should reside in the J2/1 at any given time. A check of the available data suggests that 2 such  $H < 14$  objects currently reside in the J2/1, and that the power-law index of the 11 objects with  $H < 17$  is  $\gamma \simeq 0.31$ . These values are in reasonable agreement with our results, enough that we predict the very unstable population in the J2/1 is likely to be dominated by dormant JFCs.

## 4 CONCLUSIONS

We have shown that the unstable asteroids residing in the 2/1 mean motion resonance with Jupiter have most likely been transported to their current orbits by the Yarkovsky effect; similarly we argued that objects on very unstable orbits are mostly dormant (or active) Jupiter family comets. This model satisfies several constraints: the total number of observed resonant asteroids (larger than some threshold), the slope of their power-law  $H$  distribution, and their location in phase space inside the J2/1. To further strengthen our model we need to improve our constraints or find new ones.

To add to our constraints, we need further observations (both recoveries and new discoveries) of faint asteroids in the J2/1. At the present rate of discovery, ground-based surveys may increase the population of multi-opposition resonant asteroids up to  $\simeq 500$  by the end of 2005. Advanced survey programs (e.g., Pan-STARRS) or space-borne programs

(e.g., GAIA) will further boost the rate of discoveries, such that by the end of this decade the population of known resonant asteroids might very well increase to thousands.

Our model also provides some testable predictions. For instance, we would expect the majority of asteroids on unstable orbits to have prograde rotations because Yarkovsky transport toward larger values of semimajor axis requires obliquities in the range  $0^\circ - 90^\circ$ . We can check this conclusion by testing what happens when we track the evolution of asteroid spin states (e.g., Vokrouhlický et al. 2003, 2004). This would include numerically integrating spin orientations for asteroids evolving toward the J2/1 along the orbits described in Sec. 3.1. Initially, we assume low obliquity values. When an asteroid enters the J2/1, orbital changes and interactions with various secular resonances produce chaotic evolution of the spin axis, in particular forcing the obliquity to span a large interval of values. This effectively erases the “memory” of the pre-resonance state. However, we find the rotation stays prograde in the majority of cases. Unfortunately, photometry and light-curve inversion for faint distant objects is too difficult to allow us to obtain obliquity solutions for most unstable resonant asteroids. New data from large observing programs will be needed (e.g., Kaasalainen 2004).

While the origin of the unstable asteroids in the J2/1 resonance can be partially understood by the model described above, the origin of Zhongguos and Griquas remains puzzling. We know from Sec. 2 that both islands A and B are populated, with the former significantly less than the latter. Planetary migration might be responsible for such a differential depletion of primordial populations in both islands (e.g. Ferraz-Mello et al. 1998) or even cause their secondary re-population (see the work of Morbidelli et al. (2004) for Trojan asteroids). However, a steep size distribution of B-Zhongguos make us think of a disruption which occurred recently and dominantly populated with ejecta this island. On contrary, the shallow size distribution of B-Griquas poses a problem for a model explaining them as B-Zhongguos slowly leaking by Yarkovsky effect, because such mechanism should more effectively act on smaller asteroids. We noted in Sec. 2 that the island A objects could hardly be ejecta from a disruptive event in the island B, because, for instance, the difference of mean inclination of their orbits would require ejection velocities of several km/s (a possibility is, though, that their inclination values have been later influenced by the near-by  $\nu_{16}$  secular resonance). This makes the situation even more puzzling, with possibly complex hypotheses such as recently formed population of asteroids in the island B and primordial population of asteroids in the island A.

## ACKNOWLEDGEMENTS

The work of MB and DV has been supported by the Grant Agency of the Czech Republic. We thank the referee, Kleomenis Tsiganis, for valuable comments, that improved the final version of the paper.

## REFERENCES

- Bottke W.F., Jedicke R., Morbidelli A., Petit J.-M., Gladman B., 2000, *Science*, 288, 2190
- Bottke W.F., Vokrouhlický D., Brož M., Nesvorný D., Morbidelli A., 2001, *Science*, 294, 1693
- Bottke W.F., Morbidelli A., Jedicke R., Petit J.-M., Levison H.F., Michel P., Metcalfe T.S., 2002, *Icarus*, 156, 399
- Bottke W.F., Vokrouhlický D., Rubincam D.P., Brož M., 2003, in W.F. Bottke et al., eds, *Asteroids III*, The University of Arizona Press, Tucson, p. 395
- Bottke W.F., Durda D.D., Nesvorný D., Jedicke R., Morbidelli A., Vokrouhlický D., Levison H.F., 2005, *Icarus*, in press
- Brož M., Vokrouhlický D., Roig F., Nesvorný D., Bottke W.F., Morbidelli A., 2005, in Z. Knežević and A. Milani, eds, *Dynamics of Populations of Planetary Systems*, The Cambridge University Press, Cambridge, in press
- Čapek D., Vokrouhlický D., 2004, *Icarus*, 172, 526
- Dahlgren M., 1998, *Astron. Astrophys.*, 336, 1056
- Davis D.R., Chapman C.R., Weidenschilling S.J., Greenberg R., 1985, *Icarus*, 62, 30
- Dohnanyi J.W., 1969, *J. Geophys. Res.*, 74, 2531
- Durda D.D., Greenberg R., Jedicke R., 1998, *Icarus*, 135, 431
- Eftymiopoulos C., Contopoulos G., Voglis N. 1999, *Celest. Mech. Dyn. Astron.*, 73, 221
- Farinella P., Vokrouhlický D., 1999, *Science*, 283, 1507
- Farinella P., Vokrouhlický D., Hartmann W.K., 1998, *Icarus*, 132, 378
- Ferraz-Mello S., 1994, *AJ*, 108, 2330
- Ferraz-Mello S., Michtchenko T.A., Roig F., 1998, *AJ*, 116, 1491
- Gladman B.J. et al. 1997, *Science*, 297, 177
- Guillens S.A., Vieira Martins R., Gomes R.S., 2002, *AJ*, 124, 2322
- Hagihara Y., 1975, *Celestial Mechanics*, Vol. IV, Japan Society for the promotion of Science, Tokyo
- Henrard J., Lemaître A., 1983, *Celest. Mech.*, 30, 197
- Henrard J., Lemaître A., 1987, *Icarus*, 69, 266
- Henrard J., Watanabe N., Moons, M., 1995, *Icarus*, 115, 336
- Ivezić Z. et al., 2001, *AJ*, 122, 2749
- Jedicke R., Larsen J., Spahr T., 2003, in W.F. Bottke et al., eds, *Asteroids III*, The University of Arizona Press, Tucson, p. 71
- Kaasalainen M., 2004, *A&A*, 422, L39
- Knežević Z., Lemaître A, Milani A., 2003, in W.F. Bottke et al., eds, *Asteroids III*, The University of Arizona Press, Tucson, p. 603
- Laskar J., Robutel P., 2001, *Celest. Mech. Dyn. Astr.*, 80, 39
- Lemaître A., Henrard, J., 1990, *Icarus*, 83, 391
- Levison H., Duncan M., 1994, *Icarus*, 108, 18
- Levison H., Duncan M., 1997, *Icarus*, 127, 13
- Levison H., Morbidelli A., Dones L., Jedicke R., Wiegert P.A., Bottke W.F., 2002, *Science*, 296, 2212
- Luther R., 1869, *AN*, 74, 31
- Malyshkin L., Tremaine S., 1999, *Icarus*, 141, 341
- Marzari F., Davis D., Vanzani V., 1995, *Icarus*, 113, 168
- Milani A., Farinella P., 1995, *Icarus*, 115, 209
- Milani A., Sansaturio M.E., Chesley S.R., 2001, *Icarus*, 151, 150
- Michel P., Benz W., Tanga P., Richardson D.C., 2001, *Science*, 294, 1696
- Michtchenko T.A., Ferraz-Mello S., 1997, *P&SS*, 45, 1587
- Moons M., Morbidelli A., Migliorini F., 1998, *Icarus*, 135, 458
- Morbidelli A., 1996, *AJ*, 111, 2453
- Morbidelli A., 2002, *Modern Celestial Mechanics: Aspects of Solar System Dynamics*, Taylor and Francis, London
- Morbidelli A., Moons M., 1993, *Icarus*, 102, 316
- Morbidelli A., Nesvorný D., 1999, *Icarus*, 139, 295
- Morbidelli A., Vokrouhlický D., 2003, *Icarus*, 163, 120
- Morbidelli A., Levison H.F., Tsiganis K., Gomes R.S., 2004, *Nature*, submitted
- Morbidelli A., Zappalà V., Moons M., Cellino A., Gonczi R., 1995, *Icarus*, 118, 132
- Morbidelli A., Nesvorný D., Bottke W.F., Michel P., Vokrouhlický D., Tanga P., 2003, *Icarus*, 162, 328
- Murray C.A., 1986, *Icarus*, 65, 70
- Nesvorný D., Ferraz-Mello S., 1997, *Icarus*, 130, 247
- Nesvorný D., Morbidelli A., 1998, *AJ*, 116, 3029
- Nesvorný D., Bottke W.F., 2004, *Icarus*, 170, 324
- Nesvorný D., Morbidelli A., Vokrouhlický D., Bottke W.F., Brož M., 2002a, *Icarus*, 157, 155
- Nesvorný D., Bottke W.F., Dones L., Levison H.F., 2002b, *Nature* 417, 720
- Nesvorný D., Bottke W.F., Levison H.F., Dones L., 2003, *ApJ* 591, 486
- O'Brien D.P., Greenberg R., 2003, *Icarus*, 164, 334
- Pravec P., Harris A.W., Michałowski T., 2003, in W.F. Bottke et al., eds, *Asteroids III*, The University of Arizona Press, Tucson, p. 113
- Quinn T.R., Tremaine, S., Duncan, M. 1991, *AJ*, 101, 2287
- Roig F., Nesvorný D., Ferraz-Mello S., 2002, *MNRAS*, 335, 417
- Rubincam D.P., 2000, *Icarus*, 148, 2
- Stokes G.H., Evans J.B., Larson S.M., 2003, in W.F. Bottke et al., eds, *Asteroids III*, The University of Arizona Press, Tucson, p. 45
- Tedesco E.F., Noah P.V., Noah M., Price S.D., 2002, *AJ*, 123, 1056
- Tietjen F., 1869, *AN*, 74, 47
- Tsiganis K., Varvoglis H., Morbidelli A., 2003, *Icarus*, 166, 131
- Vokrouhlický D., 1998, *A&A*, 335, 1093
- Vokrouhlický D., 1999, *A&A*, 344, 362
- Vokrouhlický D., Farinella P., 1999, *AJ*, 118, 3049
- Vokrouhlický D., Čapek D., 2002, *Icarus*, 159, 449
- Vokrouhlický D., Nesvorný D., Bottke W.F., 2003, *Nature*, 425, 147
- Vokrouhlický D., Bottke W.F., Nesvorný D., 2005, *Icarus*, in press
- Vokrouhlický D., Brož M., Farinella P., Knežević Z., 2001, *Icarus*, 150, 78
- Williams D.R., Wetherill G.W., 1994, *Icarus*, 107, 117